



A torpor-like state in mice slows blood epigenetic aging and prolongs healthspan

Received: 20 March 2024

Accepted: 3 February 2025

Published online: 7 March 2025

Check for updates

Lorna Jayne^{1,2,10}, Aurora Lavin-Peter^{1,2}, Julian Roessler¹, Alexander Tyshkovskiy¹, Mateusz Antoszewski¹, Erika Ren¹, Aleksandar Markovski¹, Senmiao Sun^{2,7}, Hanqi Yao², Vijay G. Sankaran¹, Vadim N. Gladyshev¹, Robert T. Brooke⁸, Steve Horvath¹, Eric C. Griffith¹ & Sinisa Hrvatin¹

Torpor and hibernation are extreme physiological adaptations of homeotherms associated with pro-longevity effects. Yet the underlying mechanisms of how torpor affects aging, and whether hypothermic and hypometabolic states can be induced to slow aging and increase healthspan, remain unknown. Here we demonstrate that the activity of a spatially defined neuronal population in the preoptic area, which has previously been identified as a torpor-regulating brain region, is sufficient to induce a torpor-like state (TLS) in mice. Prolonged induction of TLS slows epigenetic aging across multiple tissues and improves healthspan. We isolate the effects of decreased metabolic rate, long-term caloric restriction, and decreased core body temperature (T_b) on blood epigenetic aging and find that the decelerating effect of TLSs on aging is mediated by decreased T_b . Taken together, our findings provide novel mechanistic insight into the decelerating effects of torpor and hibernation on aging and support the growing body of evidence that T_b is an important mediator of the aging processes.

In response to food deprivation or harsh environmental conditions, many mammalian species engage energy-conserving strategies, such as torpor and hibernation. Torpor is a state of profoundly decreased metabolic rate, driving a decrease in core body temperature (T_b) that can last from hours to days, whereas hibernation is a seasonal behavior comprising multiple bouts of torpor interrupted by periodic arousals to euthermia. These extraordinary adaptations raise many unanswered fundamental questions of homeotherm biology, one of the most compelling being the link between torpor and longevity. Natural torpor is characterized by tightly coupled, extreme physiological changes that have been individually implicated in aging and longevity, such as decreased core T_b and metabolic rate, and caloric restriction. Indeed, hibernating species exhibiting long torpor bouts show extended

longevity compared to closely related non-hibernators and longer lifespan than would be expected based on body mass alone¹. However, the lack of genetic tools and controllable systems to study torpor have left the central questions of how torpor affects aging and whether hypothermic and hypometabolic states can be induced to slow aging and increase healthspan, largely unexplored.

The brain is known to control core T_b and metabolism^{2,3}. Specialized populations of neurons in the preoptic area (POA) of the hypothalamus receive information about physiological states, including peripheral and core T_b , and modulate thermoregulatory circuits to maintain homeostasis⁴⁻⁷. In addition to the role of the POA in normothermic thermoregulation, recent work has identified neuronal populations in the POA whose activity is necessary for the normal

¹Whitehead Institute for Biomedical Research and Department of Biology, Massachusetts Institute of Technology, Cambridge, MA, USA.

²Department of Neurobiology, Harvard Medical School, Boston, MA, USA. ³Division of Genetics, Department of Medicine, Brigham and Women's Hospital, Harvard Medical School, Boston, MA, USA. ⁴Division of Hematology/Oncology, Boston Children's Hospital, Harvard Medical School, Boston, MA, USA.

⁵Department of Pediatric Oncology, Dana-Farber Cancer Institute, Harvard Medical School, Boston, MA, USA. ⁶Broad Institute of MIT and Harvard, Cambridge, MA, USA. ⁷Program in Neuroscience, Harvard Medical School, Boston, MA, USA. ⁸Epigenetic Clock Development Foundation, Torrance, CA, USA. ⁹Altos Labs, Cambridge, UK. ¹⁰Present address: Department of Neurobiology, Stanford University Medical Center, Stanford, CA, USA.

e-mail: shrvatin@wi.mit.edu

expression of fasting-induced daily torpor in mice^{8,9}. Stimulation of these neurons is sufficient to induce torpor-like hypothermic and hypometabolic states^{8–11}. Building on this work, we develop a controllable torpor-like state (TLS) that can be safely maintained for days and repeatedly induced over months in non-transgenic laboratory mice. While torpor and hibernation are complex behaviors that TLS does not fully recapitulate, induction of TLS causes a profound decrease in core T_b , body temperature set point (T_{set}), metabolic rate (VO_2), respiratory quotient, activity, and food intake, phenocopying several key features of natural torpor and hibernation^{12,13}.

To examine the effects of TLS on aging, we induce prolonged TLS to model a natural hibernation-like pattern over the course of months and find that TLS improved clinical measures of age-associated frailty in mice and slowed epigenetic aging in a tissue-specific manner. TLS had the greatest effect on epigenetic aging in the blood, where it slowed epigenetic aging by up to 76% in individual mice. Moreover, we leverage the uniquely controllable nature of our model to elucidate the underlying mechanisms of the decelerating effect of TLS on blood epigenetic aging, demonstrating that this effect is not mediated by caloric restriction nor decreased metabolic rate but rather stems from a decrease in T_b .

Results

Development of an inducible TLS in non-transgenic laboratory mice

Building on recent work that has identified the POA of the hypothalamus as a torpor-regulating brain region^{8–11}, we tested whether targeted stimulation of the anterior and ventral portions of the medial and lateral preoptic area (avMLPA) of the hypothalamus could recapitulate key physiological features of torpor in non-transgenic laboratory mice.

Mice were implanted with telemetric temperature probes and stereotactically injected in the avMLPA with AAV-hSyn-hM3D(Gq)-mCherry, an adeno-associated virus (AAV) expressing a chemically activated receptor, Gq-DREADD (Gq-coupled Designer Receptor Exclusively Activated by Designer Drug), driven by the neuronally restricted *hSyn* promoter (Fig. 1a–f). Activation of neurons within the avMLPA via intraperitoneal injection of the Gq-DREADD-activating synthetic ligand clozapine-N-oxide (CNO) drove a decrease in T_b (Fig. 1a–f), consistent with targeting the avMLPA neuronal population whose activity is sufficient to induce a large decrease in T_b as observed during natural fasting-induced torpor bouts.

In mice, fasting-induced daily torpor bouts last only several hours before arousal to euthermia^{8,12,14–16}. Hibernators, by contrast, engage in torpor bouts lasting days to weeks^{17–19}. Having found that targeted chemogenetic stimulation of the avMLPA recapitulates decreases in T_b as in fasting-induced daily torpor, we tested whether this approach could be used to induce a TLS in mice lasting days to weeks, as seen in natural hibernation. Mice implanted with telemetric temperature probes and stereotactically injected in the avMLPA with AAV-hSyn-hM3D(Gq)-mCherry were continuously administered CNO via drinking water, inducing a hypothermic state that remarkably could be safely maintained for days at a time (Fig. 1g,h). To characterize and capture metabolic changes during TLS, we profiled T_b , locomotor activity (meters), food intake, metabolic rate (as measured by oxygen consumption (VO_2)), and the respiratory quotient using the Prometheon Metabolic System (Fig. 1h–l). We found that TLS caused a profound reduction across all measured parameters (**** $P < 0.0001$), similar to changes seen in fasting-induced daily torpor (Fig. 1h–l and Extended Data Fig. 1a–c). Over 4 days of TLS, the average T_b dropped by nearly 7 °C, while metabolic rate and food intake dropped by -56% and -81%, respectively (Fig. 1h–j). Upon removal of CNO from drinking water, mice spontaneously recovered across all measured metabolic parameters (Fig. 1h–l).

Natural hibernators achieve a lowered T_b during torpor by modifying key features of their thermoregulatory system, reducing both their

sensitivity to decreased T_b (H) and their theoretical set point temperature (T_{set})^{17–19}. To assess changes in these thermoregulatory parameters in TLS mice, we monitored metabolic rate (VO_2) and T_b in these animals across varied ambient temperatures (T_a) as previously described (Extended Data Fig. 2a–e)¹⁴. As animals are exposed to lower T_a , their T_b dips and their VO_2 increases to maintain a steady T_b . By measuring how the animal's VO_2 changes in response to a colder environment, we can estimate how sensitive the animal is to changes in temperature (H) and thus estimate the T_b that the animal is attempting to maintain (T_{set}). Consistent with the entry into torpor of natural hibernators, we found that both H and T_{set} were significantly reduced in TLS (Extended Data Fig. 2a–e) in TLS. Taken together, these results suggest that the thermoregulatory system during TLS shares key features with natural hibernation and fasting-induced daily torpor.

TLS slows epigenetic aging across multiple tissues

Given the links between hibernation, which comprises multiple bouts of torpor interrupted by periodic arousals to euthermia, and longevity, we tested whether TLS slows aging. Aging is characterized by progressive decline in physiological function, increased susceptibility to disease, and death. While aging is a complex phenomenon, epigenetic clocks have recently emerged as powerful molecular biomarkers of aging^{20–23}. Recent work across multiple species of natural hibernators has found that blood epigenetic aging is slowed during hibernation, suggesting that epigenetic clocks can capture torpor-related changes in aging processes^{24,25}. We induced TLS to model a natural hibernation-like pattern by repeatedly administering CNO through drinking water, resulting in bouts of TLS with periodic arousals to euthermia (Fig. 2a,b). In parallel, control mice were injected with AAV-hSyn-mCherry in the avMLPA and administered CNO concurrently with TLS mice. While on CNO, TLS mice had significantly lower T_b (30.96 ± 0.19 °C) than control mice (35.58 ± 0.02 °C) (**** $P < 0.0001$) (Fig. 2c,d). After 3 months, we analyzed the epigenetic age of the blood, liver, kidney, and cortex and found that TLS mice aged on average 80% less in the blood (* $P = 0.007$) and 20% less in the liver (* $P = 0.034$) than age-matched controls (Fig. 2e,f). In a secondary analysis, we applied additional epigenetic clocks, including two universal pan-mammalian clocks which track highly conserved epigenetic aging effects. We found that TLS mice had lower blood epigenetic age than control mice, evidencing the robustness of the effects of TLS on blood epigenetic aging (Extended Data Fig. 3a–c). Pan-tissue epigenetic clocks showed a non-statistically significant decrease in liver epigenetic age. By contrast, there was no consistent evidence of changes in epigenetic age of the kidney or cortex in TLS mice compared with age-matched controls (Fig. 2g,h and Extended Data Fig. 3a–e). Our results suggest that inducing TLS in a facultative heterotherm that does not naturally hibernate can recapitulate the effects of natural hibernation on blood epigenetic aging²⁵. While work in natural hibernators has only explored epigenetic aging of the blood²⁵ and skin²⁴, both highly replicating tissues, our work across multiple tissues suggests that hypothermic and hypometabolic states may exert highly tissue-specific effects on epigenetic aging.

Long-term induction of TLS causes a cumulative and sustained decrease in blood epigenetic age and improves healthspan

As aging is a gradual and complex process, we induced TLS over a prolonged duration to better capture its effects on both epigenetic aging and age-related decline in physiological function. We serially measured blood epigenetic age in mice after 0, 3, 6 and 9 months of TLS and compared them to control mice that were stereotactically injected in the avMLPA with AAV-hSyn-hM3D(Gq)-mCherry and administered drinking water without CNO (Fig. 3a). TLS had a linear, cumulative effect on blood epigenetic age: while at T_0 TLS and control mice had equivalent blood epigenetic age, TLS mice appeared ~3.0 ± 0.6 months younger than control mice after 9 months of TLS (Fig. 3a–c). We used a linear regression to estimate the rate of epigenetic aging over 9 months of TLS

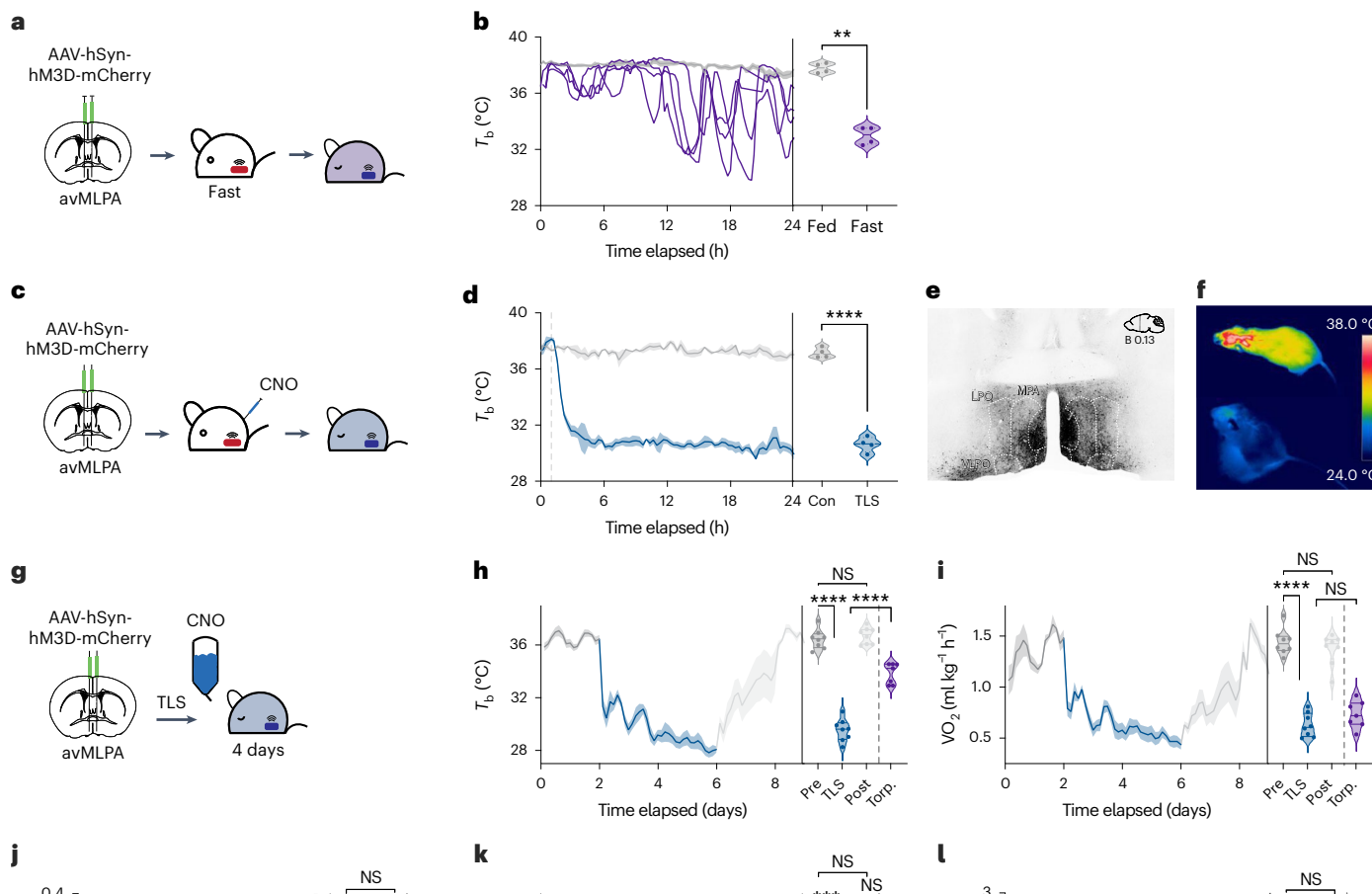


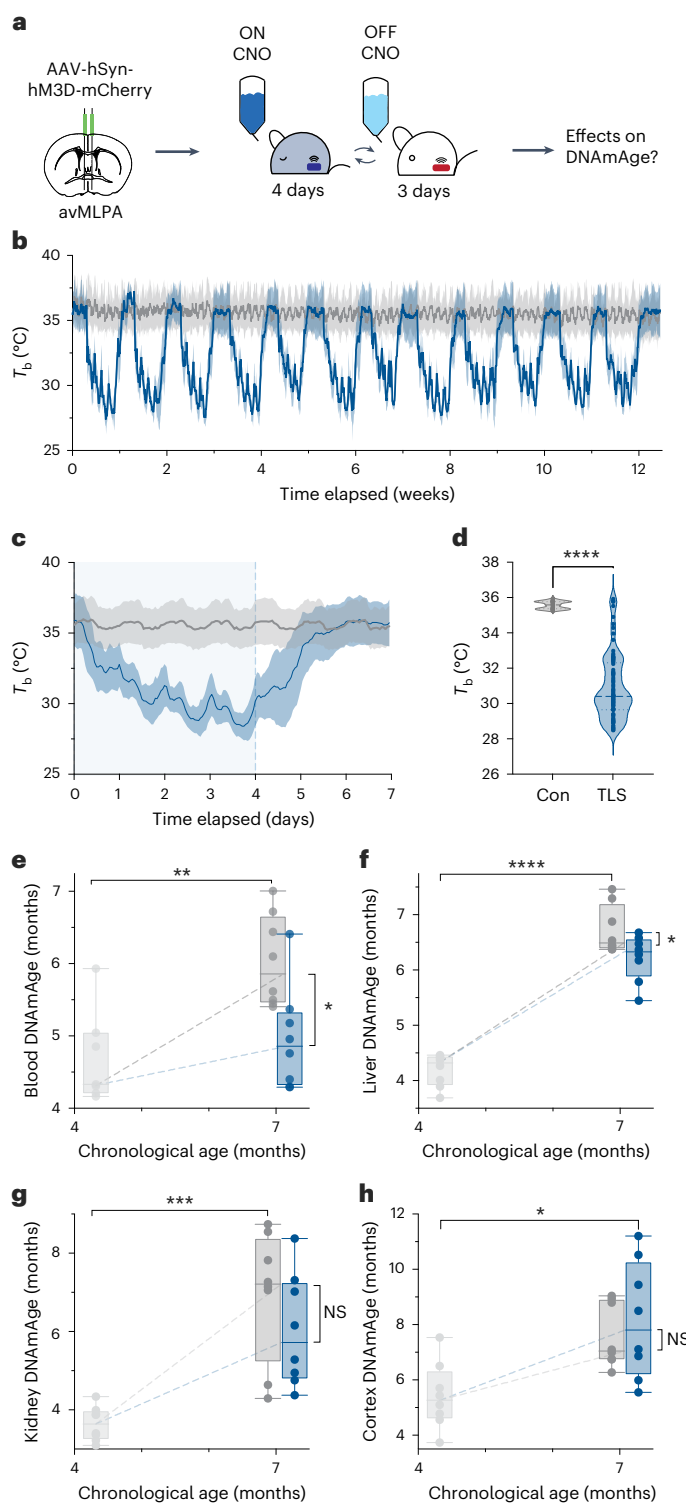
Fig. 1 | Development of an inducible TLS in non-transgenic laboratory mice. **a**, Schematic of injection of AAV-hSyn-hM3D-mCherry into the avMLPA and subsequent fasting. **b**, T_b over 24 h fasting (purple) compared to fed animals (gray). Data from fed animals plotted as mean \pm s.e.m. ($n = 4$), data from fasted animals plotted as individual mice. When fasted, all mice engaged in natural fasting-induced daily torpor as defined by $T_b < 35^\circ\text{C}$ with no arousal. Mice began engaging in torpor bouts ~ 10 h into the fasting interval. During torpor bouts, individual mice had an average T_b ($33.0 \pm 0.32^\circ\text{C}$) lower than at baseline ($37.9 \pm 0.18^\circ\text{C}$) as determined by paired t -test ($**P = 0.002$) and reported as mean \pm s.e.m. **c**, Schematic of injection of AAV-hSyn-hM3D-mCherry into the avMLPA and subsequent CNO injection. **d**, T_b after administration of CNO to mice expressing AAV-hSyn-mCherry (controls, gray), and mice injected with AAV-hSyn-hM3D-mCherry (TLS, blue) ($n = 4$). CNO injection indicated by dashed gray line. Data plotted and reported as mean \pm s.e.m. Average T_b of mice 6–24 h after CNO injection was lower in TLS animals ($30.6 \pm 0.27^\circ\text{C}$) compared to controls ($37.9 \pm 0.18^\circ\text{C}$) as determined by two-sided paired t -test ($****P < 0.0001$). **e**, Representative coronal section showing neurons in the avMLPA targeted by viral injection. hM3D expression in the avMLPA is visualized by mCherry (black) after viral injection. **f**, Thermal imaging of T_b of a mouse before (top) and after induction of TLS (bottom) illustrating the decrease in T_b that occurs during TLS. **g**, Schematic of TLS induction through continuous administration of CNO via drinking water. **h–l**, T_b (**h**), VO_2 (**i**), food intake (**j**), respiratory quotient (RQ) (**k**), and activity at baseline (dark gray) (**l**), during TLS (blue), and in recovery (light gray). Lines indicate mean; shading

denotes \pm s.e.m. ($n = 8$). Violin plots graphed as the average of each individual at baseline (Pre), during TLS (TLS), in recovery (Post), and during natural fasting-induced torpor bouts (Torp.) (purple; Extended Data Fig. 1a–c). All measured metabolic parameters had significant differences across conditions as quantified by Tukey's multiple comparisons test (T_b Pre = $36.44 \pm 0.26^\circ\text{C}$, TLS = $29.54 \pm 0.30^\circ\text{C}$, Post = $36.71 \pm 0.22^\circ\text{C}$, Torp. = $33.86 \pm 0.30^\circ\text{C}$; Pre versus Torp., $****P < 0.0001$; Torp. versus TLS, $****P < 0.0001$; Torp. versus Post, $****P < 0.0001$; Pre versus TLS, $****P < 0.0001$; Pre versus Post, NS, $P = 0.894$; TLS versus Post, $****P < 0.0001$) (VO_2 Pre = $1.44 \pm 0.04^\circ\text{C}$, TLS = $0.63 \pm 0.04^\circ\text{C}$, Post = $1.37 \pm 0.05^\circ\text{C}$, Torp. = $0.73 \pm 0.05^\circ\text{C}$; Pre versus Torp., $****P < 0.0001$; Torp. versus TLS, NS, $P = 0.324$; Torp. versus Post, $**P = 0.0026$; Pre versus TLS, $****P < 0.0001$; Pre versus Post, NS, $P = 0.6991$; TLS versus Post, $***P = 0.0003$) (Food intake Pre = 0.16 ± 0.01 , TLS = 0.03 ± 0.01 , Post = 0.20 ± 0.02 , Torp. = 0 ± 0 ; Pre versus Torp., $****P < 0.0001$; Torp. versus TLS, $**P = 0.0017$; Torp. versus Post, $****P < 0.0001$; Pre versus TLS, $****P < 0.0001$; Pre versus Post, NS, $P = 0.2259$; TLS versus Post, $***P = 0.0001$) (RQ Pre = 0.85 ± 0.01 , TLS = 0.69 ± 0.02 , Post = 0.89 ± 0.01 , Torp. = 0.67 ± 0.0 ; Torp. versus Pre, $***P < 0.0001$; Torp. versus TLS, NS, $P = 0.6233$; Torp. versus Post, $***P < 0.0001$; Pre versus TLS, $***P = 0.0004$; Pre versus Post, NS, $P = 0.1082$; TLS versus Post, $***P = 0.0004$), (Activity Pre = 1.11 ± 0.33 , TLS = 0.20 ± 0.06 , Post = 1.27 ± 0.17 , Torp. = 0.03 ± 0.02 ; Torp. versus Pre, $**P = 0.0036$; Torp. versus TLS, $*P = 0.0353$; Torp. versus Post, $***P = 0.0002$; Pre versus TLS, NS, $P = 0.0504$; Pre versus Post, NS, $P = 0.8689$; TLS versus Post, $***P = 0.0008$). Data reported as mean \pm s.e.m. m, meters.

and found that TLS reduced the rate of blood epigenetic aging by 36.9% (F -statistic (F) = 58.14, degrees of freedom for the numerator (DFn) = 1, degrees of freedom for the denominator (DFd) = 70, $****P < 0.0001$) (Fig. 3a). Longitudinal quantification of the rate of blood epigenetic aging across serial measurements from individual mice confirmed this finding; on average, individual TLS mice aged 38.9% slower than control mice (Fig. 3b). To test whether the decelerating effects of TLS are sustained, we measured blood epigenetic age in TLS mice 3 months after cessation of TLS (Fig. 3d). At this time, TLS mice still appeared -1.5 ± 0.4 months younger than control mice ($***P = 0.00013$) and did not exhibit any acceleration in epigenetic aging (Fig. 3e and Extended Data Fig. 4a). Indeed, 9 months after cessation of TLS, TLS mice still had an average blood DNAmAge (18.1 ± 1.19) -1.5 months younger than control mice (19.87 ± 0.72) (Extended Data Fig. 4b). While this difference did not reach significance (not significant (NS), $P = 0.297$), it suggests that TLS induces sustained epigenetic remodeling that was not rapidly reversed following exit from this state.

Aging causes the accumulation of physical and physiological deficits over time. Composite measures of deficit accumulation, such as the mouse clinical frailty index, serve as powerful tools to measure biological aging. Indeed, the mouse frailty index comprises 31 non-invasive measurements and is strongly correlated with and predictive of age and longevity^{26,27}. To examine whether TLS had an effect on functional measures of aging, we profiled mice using the frailty index assessment. After 9 months of TLS, TLS mice scored significantly lower on the frailty index assessment than age-matched controls ($*P = 0.0290$), indicating that they had an improved healthspan and suggesting that they were functionally younger (Fig. 3f and Extended Data Fig. 5a,b). Several individual frailty index parameters that most strongly correlate with

age ($r^2 > 0.35, P < 1 \times 10^{-30}$)²⁶ showed significant differences between TLS and control mice, including tail stiffness (* $P = 0.0463$), gait disorders (* $P = 0.043$), and kyphosis (* $P = 0.037$)²⁶, further indicating that TLS slows age-related decline in physiological function (Fig. 3g). While we cannot exclude the possibility that reverse metabolism of CNO to clozapine contributes in part to the effect of TLS on healthspan and epigenetic aging in this experiment, it is reassuring that the effects of TLS on epigenetic age are comparable in our studies controlling for CNO consumption (Figs. 2, 3a, and 4). Thus, taken together, these findings suggest that prolonged TLS slows molecular measures of aging and extend healthspan in mice.



Decreased T_b mediates the rate of blood epigenetic aging during TLS

Hibernation and TLS are complex states characterized by a host of physiological changes that have been heavily implicated in aging and longevity, most notably decreased metabolic rate, long-term caloric restriction and decreased T_b ^{28,29}. In natural states, these factors are inextricably intertwined, rendering them nearly inseparable. Here, we harnessed our inducible model of TLS to isolate the effects of decreased metabolic rate, long-term caloric restriction, and decreased T_b on blood epigenetic aging.

Metabolic rate has long been thought to modulate aging, as first explained in the ‘rate-of-living’ theory, founded on the observation that smaller animals with faster metabolisms have shorter lifespans than larger animals with slower metabolisms^{30–32}. Metabolic rate and T_b often change in parallel, making it difficult to establish a unique role for either mechanism underlying pro-longevity interventions, including natural hibernation. We sought to decouple changes in metabolism from changes in T_b during TLS by stimulating avMLPA neurons in mice housed at a thermoneutral temperature ($T_a = 32^\circ\text{C}$) to eliminate the stimulation-induced drop in T_b (Fig. 4a). We found that stimulation of the avMLPA in mice housed at thermoneutrality largely recapitulated the metabolic changes seen in TLS independent of large decreases in T_b (Fig. 4b). It is worth noting that mice at thermoneutrality exhibited a similar decrease in metabolic rate to that of mice during TLS (NS, $P = 0.1819$) (Fig. 4b).

To test whether a decrease in metabolic rate is sufficient to slow blood epigenetic aging, we repeatedly stimulated avMLPA neurons over 3 months in mice housed at thermoneutrality (Stim 32 °C), mimicking the pattern of long-term TLS (Fig. 4c,d). Stim 32 °C mice had equivalent average T_b to control mice injected with AAV-hSyn-mCherry dosed with CNO and housed at 22 °C (Con 22 °C), indicating that we were able to decouple changes in metabolic rate from changes in T_b (NS, $P = 0.9941$) (Fig. 4d and Extended Data Fig. 7a,e,f). After 3 months, we measured blood epigenetic age and found that Stim 32 °C mice had equivalent blood epigenetic age to control mice injected with AAV-hSyn-mCherry dosed with CNO when housed at 22 °C (No Stim 22 °C) (NS, $P = 0.9961$) and at 32 °C (No Stim 32 °C) (NS, $P = 0.7848$) (Fig. 4e). Stim 32 °C mice had significantly higher blood epigenetic age than TLS mice (* $P = 0.0309$) (Fig. 4e), indicating that decreased

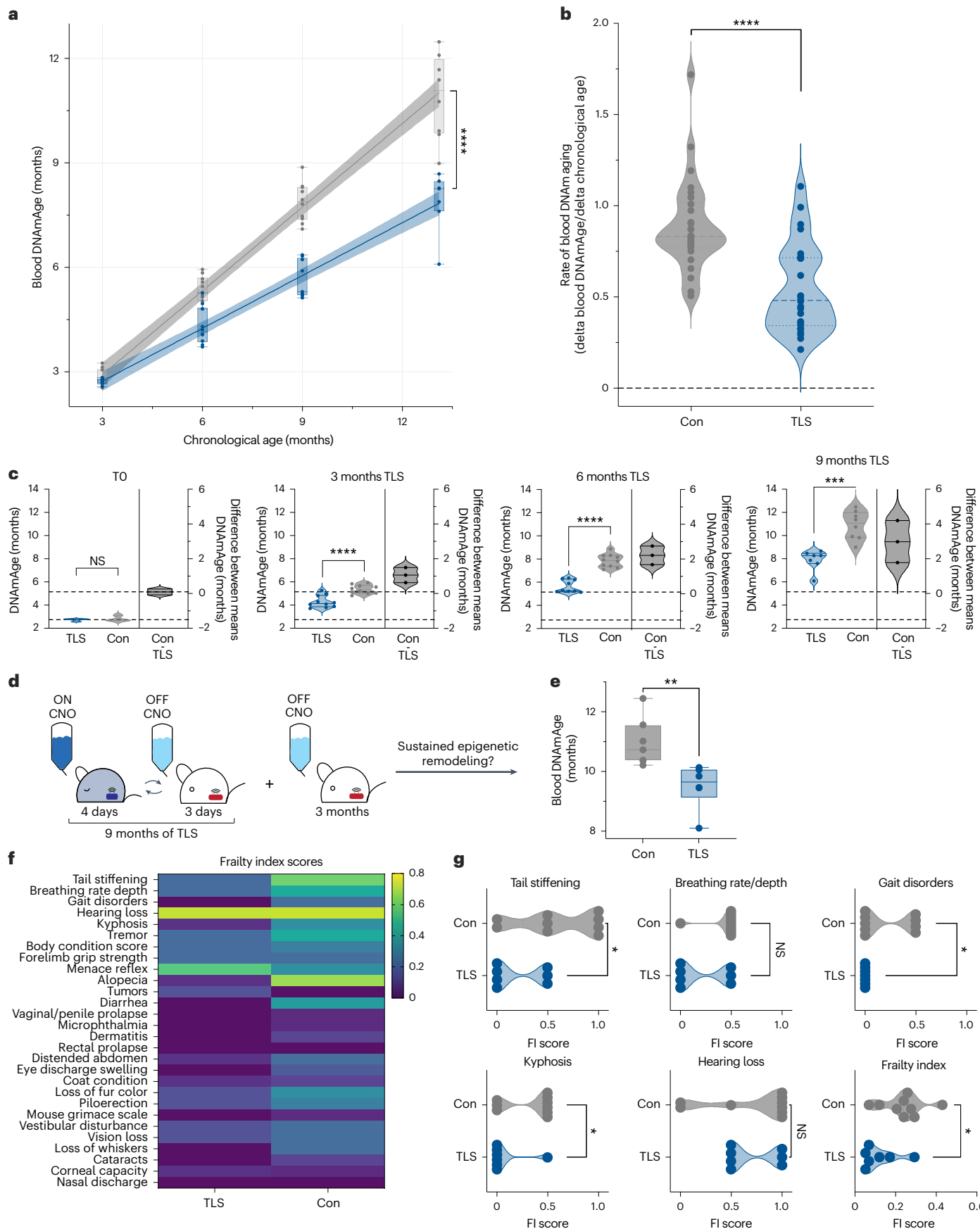
metabolic rate alone is not sufficient to reproduce the decelerating effects of TLS on blood epigenetic aging.

Having found that decreased metabolic rate was insufficient to recapitulate the effects of TLS on blood epigenetic aging, we tested whether caloric restriction underlies the decelerating effects of TLS. Caloric restriction is one of the most well-known and effective anti-aging interventions shown to extend lifespan across species³³. Caloric restriction in mice results in time-restricted feeding and long fasting intervals during which mice routinely enter torpor, as characterized by decreases in T_b ³⁴. To isolate the effects of caloric restriction independent of drops in T_b during fasting-induced daily torpor, mice injected with AAV-hSyn-mCherry were housed at thermoneutrality, dosed with CNO through drinking water, and pair-fed to match food intake in TLS mice (0.95 g d⁻¹) (CR 32 °C; CR, caloric restriction) (Fig. 4f and Extended Data Fig. 7a–d,g,h). CR 32 °C mice had similar average T_b to No Stim 22 °C mice, indicating that we were able to isolate the effects of caloric restriction from T_b (NS, $P = 0.9030$) (Fig. 4g and Extended Data Fig. 7a,b,g,h). After 3 months, CR 32 °C mice had equivalent blood epigenetic age to both No Stim 22 °C mice (NS, $P = 0.9990$) and No Stim 32 °C mice (NS, $P = 0.7893$) (Fig. 4h). CR 32 °C mice had significantly higher blood epigenetic age than TLS mice (** $P = 0.0004$) (Fig. 4h), suggesting that caloric restriction in the absence of T_b decreases during natural fasting-induced daily torpor is not sufficient to recapitulate the effects of TLS on blood epigenetic aging.

Given that caloric restriction and decreased metabolic rate on their own were insufficient to slow blood epigenetic aging, we hypothesized that decreased T_b was necessary for the decelerating effects of TLS on epigenetic aging. To isolate the effect of decreased T_b during TLS on blood epigenetic aging, we housed mice at thermoneutrality and both stimulated avMLPA neurons and pair-fed them with TLS mice (Stim + CR 32 °C) (Fig. 4i and Extended Data Fig. 7a–d,i,j). Stim + CR 32 °C mice thus exhibited both a decreased metabolic rate and long-term caloric restriction independent of large decreases in T_b . Stim + CR 32 °C mice had equivalent average T_b to No Stim 22 °C mice (NS, $P = 0.9915$), indicating that we were able to blunt large decreases in T_b characteristic of TLS (Fig. 4j and Extended Data Fig. 7a,i). After 3 months, we measured blood epigenetic age and found that Stim + CR 32 °C mice had equivalent blood epigenetic age to both No Stim 22 °C mice (NS, $P = 0.6854$) and No Stim 32 °C mice (NS, $P > 0.9999$) (Fig. 4k).

Fig. 3 | Long-term induction of TLS causes a cumulative and sustained decrease in blood epigenetic age and improves healthspan. **a**, Blood epigenetic age was serially measured every 3 months in control (gray) and TLS (blue) mice over 9 months. Both control and TLS mice were injected with pAAV-hSyn-Hm3D(GQ)-mCherry. TLS mice received repeated CNO administration, while control mice received water. Data plotted as box plots (25th to 75th percentiles) with whiskers from minimum to maximum with line at median. Simple linear regression was used to calculate the rate of blood epigenetic aging over 9 months; line represents regression; shading denotes 95% confidence interval (CI). TLS mice had a significantly slower rate of blood epigenetic aging 0.51 [0.46, 0.56] ($r^2 = 0.924$, *** $P < 0.0001$) than control mice 0.81 [0.74, 0.86] ($r^2 = 0.953$, *** $P < 0.0001$) ($F = 58.14$, DFn = 1, DFd = 70, *** $P < 0.0001$) over 9 months of TLS. Data reported as mean with 95% CI in brackets. **b**, Quantification of the average rate of epigenetic aging measured every 3 months for 9 months across individual mice. TLS mice had a significantly slower rate of epigenetic aging ($n = 26$, 0.545 ± 0.047) as determined by two-tailed unpaired t-test than control mice ($n = 26$, 0.892 ± 0.05) (** $P < 0.0001$). Data reported as mean \pm s.e.m. **c**, Estimation plots of the difference between means of TLS and control mice across measured time points. Data reported as mean \pm s.e.m. Significance determined by unpaired two-tailed t-tests. Before treatment began (T_0), control (2.83 ± 0.075) and TLS (2.74 ± 0.03) mice had equivalent blood epigenetic age (control $n = 11$, 6 female mice, 5 male mice; TLS $n = 10$, 6 female mice, 4 male mice) (NS, $P = 0.252$). After 3, 6 and 9 months of TLS, TLS mice had increasingly lower mean epigenetic age than controls (at 3 months, TLS = 4.31 ± 0.168 , Con = 5.37 ± 0.121 , *** $P < 0.0001$ (control $n = 11$, 6 female mice, 5 male mice;

TLS $n = 10$, 6 female mice, 4 male mice); at 6 months, TLS = 5.67 ± 0.180 , Con = 7.87 ± 0.178 , *** $P < 0.0001$ (control $n = 10$, 6 female mice, 4 male mice; TLS $n = 9$, 6 female mice, 3 male mice); at 9 months, TLS = 7.90 ± 0.330 , Con = 10.89 ± 0.434 , ** $P = 0.0001$ (control $n = 8$, 6 female mice, 2 male mice; TLS, $n = 7$, 5 female mice, 2 male mice). **d**, Schematic of testing for sustained epigenetic remodeling. After 9 months of TLS, mice were off CNO for 3 months, after which time blood epigenetic age was measured again. **e**, Quantification of blood epigenetic age 3 months post-TLS. Data plotted as box plots (25th to 75th percentiles) with whiskers from minimum to maximum with line at median. TLS mice (9.51 ± 0.305) still had significantly younger blood epigenetic age than control mice (10.96 ± 0.305), (** $P = 0.0065$) (control $n = 7$, 5 female mice, 2 male mice; TLS $n = 6$, 4 female mice, 2 male mice) as determined by two-tailed unpaired t-test. Data reported as mean \pm s.e.m. **f**, Heat map of the average scores on frailty index measurements of TLS and control mice after 9 months of TLS ($n = 7$). Frailty index measurements are arranged in decreasing order of strongest correlation with age. **g**, Violin plots of frailty index scores of TLS mice and control mice on the five individual frailty index measurements that most strongly correlate with age and overall frailty index score. TLS mice scored significantly lower than control mice as determined by two-tailed unpaired t-test (TLS $n = 7$, 5 female mice, 2 male mice; control $n = 9$, 6 female mice, 3 male mice) on tail stiffening (TLS = 0.214 ± 0.101 , Con = 0.611 ± 0.139 , * $P = 0.0463$), gait disorders (TLS = 0 ± 0 , Con = 0.222 ± 0.088 , * $P = 0.043$), and kyphosis (TLS = 0.071 ± 0.071 , Con = 0.333 ± 0.083 , * $P = 0.037$), as well as overall frailty index score (TLS = 0.118 ± 0.034 , Con = 0.238 ± 0.035 , * $P = 0.0290$). Data reported as mean \pm s.e.m. FI, frailty index.



Stim + CR 32 °C mice had significantly higher blood epigenetic age than TLS mice, ($*P = 0.0108$), indicating that despite having both a decreased metabolic rate and undergoing long-term caloric restriction, Stim + CR 32 °C mice do not recapitulate the effects of TLS on blood epigenetic aging (Fig. 4k). Differential methylation analysis further supported the temperature dependence of epigenetic remodeling during TLS (Extended Data Fig. 9a–l). Taken together, our results show the insufficiency of caloric restriction and decreased metabolic rate, both alone and when combined, to recapitulate the effects of TLS on blood epigenetic age, thus pointing to decreased T_b as necessary for the decelerating effects of TLS on blood epigenetic aging.

In light of the necessity of decreased T_b to capture the effects of TLS on blood epigenetic aging, we took advantage of the variability in the depth of TLS across individual animals by comparing the rate of blood epigenetic aging to the average decrease in T_b while on CNO over 9 months of TLS (Fig. 4l–n). This analysis revealed a significant correlation ($r^2 = 0.5869$, $****P < 0.0001$) between the average decrease in T_b and the rate of epigenetic aging across control and TLS mice (Fig. 4m). There was no significant correlation between the average decrease in T_b while on CNO and bodyweight, or between bodyweight and the rate of blood epigenetic aging (Extended Data Fig. 6). We further examined

whether sex had an effect on the rate of epigenetic aging in TLS and found no sex differences within groups across experiments (Extended Data Fig. 8). Taken altogether, our results suggest that temperature might play a central role in mediating the rate of epigenetic aging. The correlation between the rate of epigenetic aging and the average decrease in T_b held significance in TLS mice alone ($r^2 = 0.2428$, $*P = 0.0321$), further supporting the hypothesis that decreases in T_b might mediate the effect of TLS on blood epigenetic aging (Fig. 4n).

In summary, we show that long-term induction of a TLS through targeted stimulation of the avMLPA has decelerating effects on both functional and epigenetic measures of aging. While not possible in natural torpor or hibernation, we took advantage of the controllable nature of TLS to show that neither caloric restriction nor lower metabolic rate are sufficient and that instead decreased core T_b is necessary for TLSs to slow blood epigenetic aging.

Discussion

Our study examines the age-decelerating effects of hypothermic and hypometabolic states, such as torpor and hibernation, which are extreme physiological adaptations of homeotherms. While there are well-established links between hibernation, composed of multiple

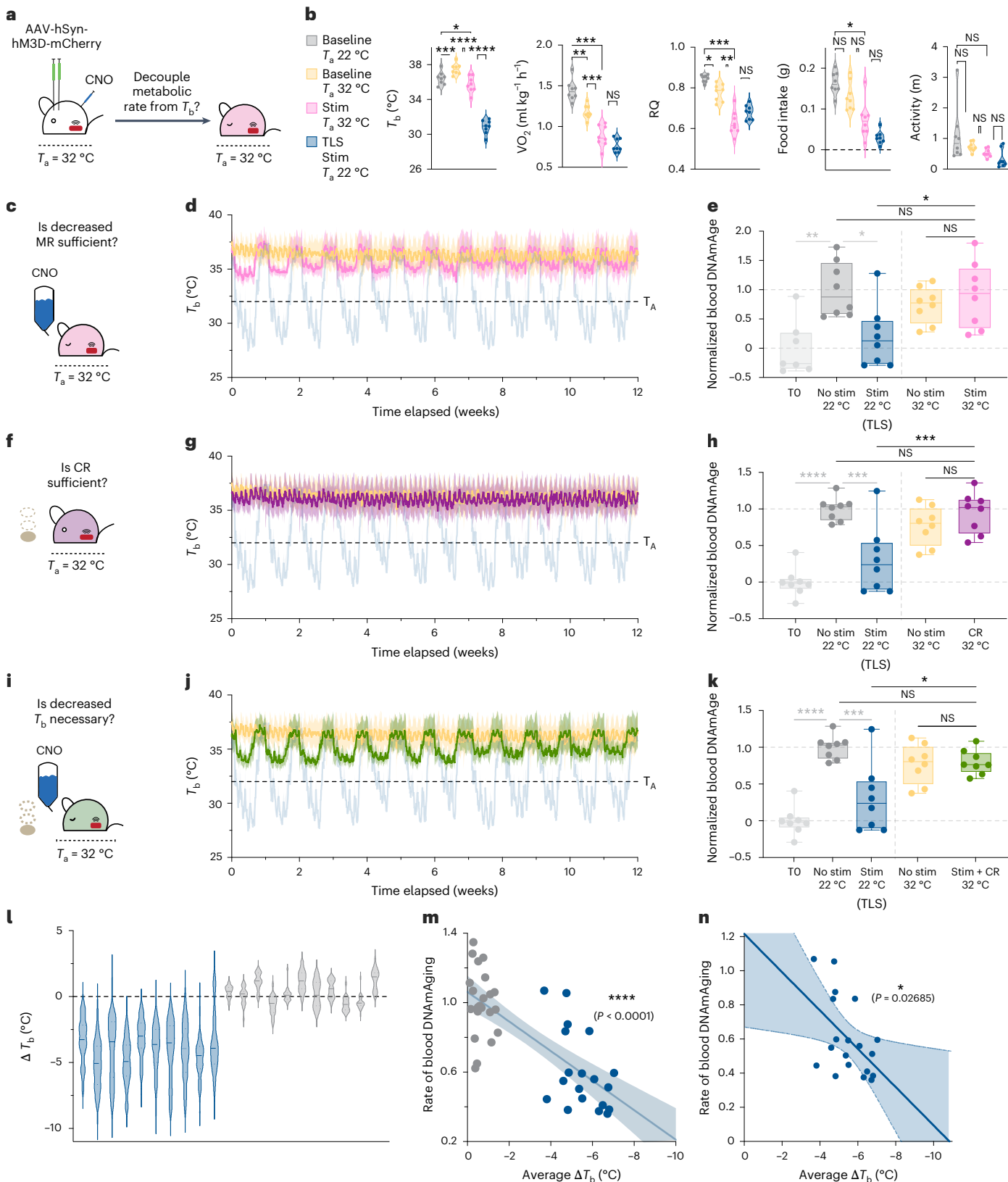
Fig. 4 | Decreased T_b mediates the rate of blood epigenetic aging during TLS.

a, Schematic of stimulating avMLPA neurons while housing mice at thermoneutrality ($T_a = 32$ °C) to decouple changes in metabolic rate from changes in temperature. **b**, Quantification of T_b , metabolic rate (VO_2), respiratory quotient (RQ), food intake, and activity of mice at baseline and during stimulation of the avMLPA while housed at thermoneutrality ($T_a = 32$ °C) compared to mice at baseline and in TLS ($T_a = 22$ °C). Data plotted as the average of each individual mouse and reported as mean ± s.e.m. Significance determined by one-way ANOVA adjusted for multiple comparisons by Tukey's HSD (T_b , Baseline T_a 22 °C = 36.44 ± 0.26 , Baseline T_a 32 °C = 37.50 ± 0.22 , Stim T_a 32 °C = 35.73 ± 0.32 , TLS (Stim T_a 22 °C) = 30.85 ± 0.28 ; TLS Stim T_a 22 °C versus Stim T_a 32 °C, $****P < 0.0001$; TLS Stim T_a 22 °C versus Baseline T_a 22 °C, $****P < 0.0001$; TLS Stim T_a 22 °C versus Baseline T_a 32 °C, $****P < 0.0001$; Stim T_a 32 °C versus Baseline T_a 22 °C, $*P = 0.0295$; Stim T_a 32 °C versus Baseline T_a 32 °C, $****P < 0.0001$; Baseline T_a 22 °C versus Baseline T_a 32 °C, $****P < 0.0001$, (VO_2 Baseline T_a 22 °C = 1.44 ± 0.04 , Baseline T_a 32 °C = 1.17 ± 0.03 , Stim T_a 32 °C = 0.88 ± 0.05 , TLS (Stim T_a 22 °C) = 0.78 ± 0.03 ; TLS Stim T_a 22 °C versus Stim T_a 32 °C, NS, $P = 0.1819$; TLS Stim T_a 22 °C versus Baseline T_a 22 °C, $****P < 0.0001$; TLS Stim T_a 22 °C versus Baseline T_a 32 °C, $****P = 0.0001$; Stim T_a 32 °C versus Baseline T_a 22 °C, $***P = 0.0004$; Stim T_a 32 °C versus Baseline T_a 32 °C, $***P = 0.0003$; Baseline T_a 22 °C versus Baseline T_a 32 °C, $**P = 0.0012$), (RQ Baseline T_a 22 °C = 0.85 ± 0.01 , Baseline T_a 32 °C = 0.78 ± 0.02 , Stim T_a 32 °C = 0.63 ± 0.02 , TLS (Stim T_a 22 °C) = 0.68 ± 0.01 ; TLS Stim T_a 22 °C versus Stim T_a 32 °C, NS, $P = 0.1353$; TLS Stim T_a 22 °C versus Baseline T_a 22 °C, $****P < 0.0001$; TLS Stim T_a 22 °C versus Baseline T_a 32 °C, $*P = 0.0104$; Stim T_a 32 °C versus Baseline T_a 22 °C, $**P = 0.0002$; Stim T_a 32 °C versus Baseline T_a 32 °C, $**P = 0.0025$; Baseline T_a 22 °C versus Baseline T_a 32 °C, $*P = 0.0101$), (Activity Baseline T_a 22 °C = 1.11 ± 0.33 , Baseline T_a 32 °C = 0.73 ± 0.06 , Stim T_a 32 °C = 0.52 ± 0.05 , TLS (Stim T_a 22 °C) = 0.33 ± 0.10 , TLS Stim T_a 22 °C versus Stim T_a 32 °C, NS, $P = 0.4208$; TLS Stim T_a 22 °C versus Baseline T_a 22 °C, NS, $P = 0.0627$; TLS Stim T_a 22 °C versus Baseline T_a 32 °C, NS, $P = 0.0674$; Stim T_a 32 °C versus Baseline T_a 22 °C, NS, $P = 0.3760$; Stim T_a 32 °C versus Baseline T_a 32 °C, NS, $P = 0.0702$; Baseline T_a 22 °C versus Baseline T_a 32 °C, NS, $P = 0.6862$), (Food Intake Baseline T_a 22 °C = 0.16 ± 0.01 , Baseline T_a 32 °C = 0.13 ± 0.01 , Stim T_a 32 °C = 0.073 ± 0.02 , TLS (Stim T_a 22 °C) = 0.03 ± 0.01 , TLS Stim T_a 22 °C versus Stim T_a 32 °C, NS, $P = 0.0760$; TLS Stim T_a 22 °C versus Baseline T_a 22 °C, $****P < 0.0001$; TLS Stim T_a 22 °C versus Baseline T_a 32 °C, $***P = 0.0005$; Stim T_a 32 °C versus Baseline T_a 22 °C, $*P = 0.0206$; Stim T_a 32 °C versus Baseline T_a 32 °C, NS, $P = 0.0711$; Baseline T_a 22 °C versus Baseline T_a 32 °C, NS, $P = 0.1285$). **c**, Schematic of experimental design to determine sufficiency of decreased metabolic rate for effects on epigenetic aging. **d**, T_b over 12 week experiment of mice undergoing stimulation of avMLPA neurons while housed at thermoneutrality (Stim 32 °C, $n = 7$, 4 female mice, 3 male mice) plotted in pink and control non-stimulated mice housed at thermoneutrality (No Stim 32 °C, $n = 8$, 4 female mice, 4 male mice) plotted in orange. No Stim 32 °C and No Stim 22 °C mice were injected with

pAAV-hSyn-mCherry and administered CNO. T_b of TLS mice shown in blue for reference (as previously shown in Fig. 2b); lines represent means; shading denotes s.d. **e**, To compare changes in epigenetic aging across experiments, blood DNAmAge was normalized to $T_0 = 0 \pm 0.176$ and No Stim 22 °C = 1 ± 0.166 (shown for reference, previously shown in Fig. 2b); data plotted as box plots (25th to 75th percentiles) with whiskers from minimum to maximum with line at median; data reported as mean ± s.e.m. Significance determined by one-way ANOVA adjusted for multiple comparisons by Tukey's HSD. Stim 32 °C (0.911 ± 0.198) ($n = 7$, 4 female mice, 3 male mice) had similar blood epigenetic age to No Stim 32 °C mice ($n = 8$, 4 female mice, 4 male mice) (0.737 ± 0.11) (NS, $P = 0.9475$) and No Stim 22 °C mice ($n = 8$, 4 female mice, 4 male mice) (1.00 ± 0.166) (NS, $P = 0.9955$). Stim 32 °C had higher blood epigenetic age than TLS mice ($n = 8$, 4 male mice, 4 female mice) (previously shown in Fig. 2b); (0.203 ± 0.188) ($*P = 0.0394$). **f**, Schematic of experimental design to determine sufficiency of caloric restriction for effects on epigenetic aging. **g**, T_b over a 12-week experiment of mice pair-fed with TLS mice while housed at thermoneutrality (CR 32 °C, $n = 8$, 4 female mice, 4 male mice) plotted in purple. CR 32 °C mice were injected with pAAV-hSyn-mCherry and received CNO. T_b of No Stim 32 °C mice (orange) and TLS mice (blue) shown for reference (as previously shown in **d**). Lines and shading as in **d**. **h**, Quantification of normalized blood DNAmAge of CR 32 °C mice. Data plotted as box plots (25th to 75th percentiles) with whiskers from minimum to maximum with line at median. Normalization performed as in **e** ($T_0 = 0 \pm 0.069$, No Stim 22 °C = 1 ± 0.057). CR 32 °C mice had similar blood epigenetic age to No Stim 22 °C mice (NS, $P = 0.9990$) and No Stim 32 °C mice (NS, $P = 0.7893$) and significantly higher epigenetic age than TLS mice ($***P = 0.0004$) (shown for reference, as previously shown in Fig. 2b). **i**, Schematic of experimental design to determine the necessity of decreased T_b for effects on epigenetic aging. **j**, T_b over 12 week experiment of mice pair-fed with TLS mice and undergoing avMLPA stimulation housed at 32 °C (Stim + CR 32 °C, $n = 8$, 4 female mice, 4 male mice) plotted in green. T_b of No Stim 32 °C mice (orange) and TLS mice (blue) shown for reference (as shown in **d**). Lines and shading as in **h**. **k**, Quantification of normalized blood DNAmAge of Stim + CR 32 °C mice. Data plotted as box plots (25th to 75th percentiles) with whiskers from minimum to maximum with line at median. Normalization performed as in **e**. Stim + CR 32 °C mice (0.798 ± 0.058) had similar blood DNAmAge to No Stim 32 °C mice (NS, $P > 0.9999$) and No Stim 22 °C mice (NS, $P = 0.6854$). Stim + CR 32 °C mice had significantly higher blood epigenetic age than TLS mice ($*P = 0.0108$) (shown for reference, as previously shown in Fig. 2b). **l**, ΔT_b of individual control and TLS mice while on CNO over 9 months (mice previously shown in Fig. 3a). **m**, Correlation between the average ΔT_b and the rate of blood DNAmAging in individual Con 22 °C (gray) and TLS (blue) mice over 9 months ($r^2 = 0.5650$, $****P < 0.0001$, $F = 50.65$, DF_n, DF_d = 1, 17); line represents simple linear regression; shading denotes 95% CI. **n**, Correlation between the average ΔT_b and the rate of blood DNAmAging in TLS mice over 9 months ($r^2 = 0.2567$, $*P = 0.0269$, $F = 5.871$, DF_n, DF_d = 1, 17). Data shown as in **m**.

bouts of torpor, and longevity, how torpor and hibernation affect aging remains largely unexplored due to difficulties in studying natural hibernators. We demonstrate that the activity of a spatially defined neuronal population in the avMLPA, which has previously been identified as a torpor-regulating brain region, is sufficient to induce a TLS in mice. TLS shares key metabolic and thermoregulatory features with both

fasting-induced daily torpor and hibernation, namely, a decrease in metabolic rate and T_{set} . We harnessed our model of TLS to explore the effects of torpor on aging and found that, similar to natural hibernation, TLS slows blood epigenetic aging. The effects of TLS on blood epigenetic age are both cumulative and sustained, agreeing with work performed in natural hibernators that found that the length of time



spent in hibernation positively correlates with longevity, as measured by lifespan³⁵. Long-term induction of TLS increased healthspan, measured using the mouse frailty index assessment, indicating that TLS has systemic and functional effects on aging processes. We went on to leverage the controllable nature of TLS to isolate the effects of decreased metabolic rate, long-term caloric restriction, and decreased T_b on blood epigenetic aging. We found that a decrease in T_b is necessary to slow blood epigenetic aging during TLS and that the rate of blood epigenetic aging is mediated by the degree of decrease in T_b . Neither a decrease in metabolic rate nor caloric restriction, alone or combined, were sufficient to recapitulate the decelerating effects of TLS on blood epigenetic age. Our finding that decreased T_b mediates these effects of TLS agrees with recent work showing that T_b is a more important modulator of lifespan than metabolic rate²⁹. Similarly, our finding that caloric restriction independent of a decrease in T_b does not slow blood epigenetic aging agrees with the previous finding that housing mice at thermoneutrality blunts the pro-longevity effects of caloric restriction³⁶. Recent work on caloric restriction has shown that the lifespan extension effects of caloric restriction are primarily mediated by fasting intervals of >12 h during which mice likely enter torpor, reaffirming the possibility that torpor and decreased core T_b play a central role in caloric-restriction-mediated effects on longevity³⁷. Decreases in T_b have previously been correlated with increased lifespan in transgenic mice²⁸. Our finding that decreased T_b is necessary to slow blood epigenetic aging during TLS further supports the growing body of evidence that T_b is an important mediator of aging processes.

It is important to recognize the limitations of this study. In this regard, it is striking that in our longitudinal data we see a correlation between the decrease in core T_b in TLS and the rate of epigenetic aging in individual mice. Given the necessity of decreased temperature for the effects of TLS on epigenetic aging (Fig. 4k), we believe that temperature is the key mediator of this effect. However, recent work has suggested that clozapine can independently contribute to an effect on aging biomarkers^{38–40}. The effects of TLS on epigenetic age in these longitudinal experiments are comparable to those observed in our other studies that control for CNO consumption (Figs. 2 and 4), suggesting that any effects due to the reverse metabolism of CNO to clozapine are minimal. Yet, we cannot currently exclude a possible contribution role for clozapine in this aspect of our findings (Fig. 3). Separately, it is noteworthy that the frailty index measures we report in both TLS mice and controls are elevated compared to those previously reported for mice of a similar age²⁶. This may be due to several factors, including differences in scoring between experimenters and the stressors faced by both control and TLS mice, including stereotactic and abdominal surgery and repeated tail bleedings at 3, 6, and 9 months of age before frailty testing. It thus remains possible that a protective effect of TLS for stressor-induced frailty may also contribute to the observed TLS-mediated increases in healthspan. Future studies that isolate core T_b , caloric restriction, and metabolic rate while monitoring TLS-mediated effects on age-associated frailty absent these invasive techniques will be informative. Whenever possible, we used the same number of male and female mice; however, our study is not sufficiently powered to robustly detect sex-specific differences. Finally, our current analysis may underestimate the sustained nature of aspects of these TLS effects. In this regard, it is notable that the control animal cohort showed an unexplained deviation in blood epigenetic age relative to their trend line at 3 months post-TLS that would tend to minimize the sustained effects of TLS (Extended Data Fig. 4a).

It is also important to recognize that torpor and hibernation are complex behaviors involving profound physiological changes that are not fully recapitulated in our model. In light of the necessity of decreased T_b for the effects of TLS on blood epigenetic aging, and the correlation between the depth of TLS and the rate of blood epigenetic aging, perhaps the most salient difference between TLS and natural hibernation is that mice in TLS exhibit shallower drops in T_b than some

natural hibernators, who drop their T_b as low as 4 °C. While TLS captures meaningful changes in both epigenetic aging and healthspan, TLS may not reproduce pro-longevity effects that might occur from the more extreme drops of T_b in natural hibernators. Future studies in natural hibernators should address the role of extreme drops in T_b in torpor-mediated increases in longevity.

Uncovering tissue-specific aging processes is critical to understanding the age-related decline of different organs and diverse cell types. We found that while TLS has systemic effects on functional measures of aging, TLS exerts tissue-specific effects on epigenetic aging whereby induction of TLS had greater effects on tissues with higher rates of basal cell turnover, most notably the blood. It is well known that temperature is a regulator of mammalian cell cycle, whereby moderate hypothermia arrests mitosis^{41,42}. Our work showing the temperature dependence of blood epigenetic aging coupled with the observation that there is a correlation between the rate of basal cell turnover in profiled tissues and the effect size of TLS on epigenetic aging offers a working framework for the observed tissue-specific effects of TLSs on aging that future studies should further address.

Methods

Mice

Experiments performed at Harvard Medical School were approved by the National Institute of Health and Harvard Medical School Institutional Animal Care and Use Committee. Experiments performed at the Whitehead Institute at the Massachusetts Institute of Technology were approved by the National Institute of Health and the Division of Comparative Medicine and the Committee on Animal Care. All experiments followed ethical guidelines described in the US National Institutes of Health Guide for the Care and Use of Laboratory Animals and were performed using adult C57BL/6J mice (The Jackson Laboratory, stock 000664). Unless otherwise noted, all mice were group-housed at 22 °C under a standard 12 h light/dark cycle and fed ad libitum. Relative humidity was maintained at 50 ± 15% across all experiments. No statistical methods were used to predetermine sample size of groups, and unless otherwise noted, all groups contained equal numbers of male and female mice randomly assigned to experimental groups before surgery. Across all experiments, mice were between 16 and 20 weeks old at the start of the experiment.

Telemetric monitoring of core T_b

Mice were implanted with wireless probes (UID catalog number UCT-2112, Temperature Microchip) in the intraperitoneal space. Mice were allowed to recover for at least 4 days before recording. To record core T_b , cages were placed on the UID Mouse Matrix reader plate, allowing continuous and undisturbed tracking of core T_b . Unless otherwise noted, core T_b was logged every 30 s. For longitudinal experiments (Fig. 3), temperature was recorded at least three times per week using a UID handheld reader. For calculations of average temperature when temperature was taken more than once in a week while on CNO, the minimum temperature taken on CNO was used.

Viral constructs

pAAV-hSyn-mCherry (Addgene catalog number 114472-AAV8) and pAAV-hSyn-hM3D(Gq)-mCherry (Addgene catalog number 50474-AAV8) were obtained from Addgene. All AAVs were packaged by the Boston Children's Hospital Viral Core in serotype AAV8. All viruses were diluted with PBS to a final concentration between 1 and 5×10^{13} genome copies per ml before stereotaxic delivery.

Stereotactic viral injection

Stereotactic surgery was performed when mice were between 8 and 14 weeks of age. Mice were anesthetized via isoflurane inhalation and placed in a stereotactic headframe (Kopf Instruments). For all injections, coordinates AP + 0.4 mm, ML ± 0.5 mm, DV – 5 mm relative to

bregma were used to target the avMLPA. An air-based injection system was used to infuse the virus at a rate of approximately 100 nl min⁻¹, and the needle was kept at the injection site for 5 min before withdrawing. For mice singly injected, 100–150 nl of virus was bilaterally injected. For mice co-injected, viruses were mixed before injection in a 1:1 ratio, and 100–150 nl of virus was injected bilaterally.

Fasting-induced daily torpor induction

Adult mice ($n = 4$ female mice) were singly housed before food removal at a T_a of 22 °C. Food was removed at the beginning of the dark cycle, and initial bouts of torpor were seen in mice after approximately 10 h of fasting. Natural torpor was defined by a T_b of <35 °C and lack of arousal. Food was returned to cages 24 h after the start of the fast.

CNO administration

CNO solution was prepared by initially dissolving CNO hydrochloride (Sigma-Aldrich, SML2304) in H₂O to a stock solution of 100 mM. For intraperitoneal injection of CNO, the stock solution was diluted with PBS to a final concentration of 0.6 mM, and approximately 250 µl was injected intraperitoneally per mouse for a final injection concentration of 2 mg kg⁻¹. For continuous CNO administration, CNO was taken from a 100 mM stock solution and diluted in water to a final concentration between 0.01 mM and 0.04 mM.

Image analysis

Mice were anesthetized via inhalation of isoflurane and euthanized by transcardial perfusion of 10 ml PBS followed by 10 ml of 4% paraformaldehyde. Brains were extracted, post-fixed overnight with 4% paraformaldehyde at 4 °C, and then embedded in PBS with 3% agarose. Brains were sliced on a vibratome (Leica VT1200S) into 50 µm coronal sections. Sections were imaged on a TissueFax SL Q 60 µm confocal disk slide scanner using a 10 × 0.3 objective with extended focus and z-stacking.

Metabolic measurements

Mice ($n = 4$ male mice, 4 female mice) were implanted abdominally with telemetric temperature probes (Starr Life Science VV-EMITT-G2) and placed in the Sable Systems Promethion Core Metabolic System. Mice were given 24 h to acclimate before baseline recordings (2 days), followed by CNO water administration (5 days) and recovery (3 days). Data were logged every 3 min. For analysis of natural torpor, mice were fasted as described previously. Six out of eight mice underwent natural fasting-induced daily torpor bouts as defined by $T_b < 35$ °C and lack of arousal. For downstream analysis, the average value of metabolic parameters for each individual mouse was calculated across all torpor bouts.

Statistical analysis of the thermoregulatory system

To analyze the thermoregulatory system during TLS and at baseline, parameters G , T_{set} , and H were estimated from observing T_b and VO₂ across varying T_a (8, 16, 24 °C) as previously described^{10,14}. Mice ($n = 11$, 5 female mice, 6 male mice) were placed in Sable Systems Promethion Core Metabolic System for measurement of T_b and VO₂. To record baseline and TLS data, mice were intraperitoneally injected with PBS and CNO, respectively, and T_a was lowered every 3 h (24, 16, 8 °C). The minimum VO₂ and corresponding T_b , theoretically corresponding to a metabolically stable state, of each individual mouse at each temperature were used in downstream analyses.

Long-term TLS induction

Group-housed 16-week-old mice were injected with either pAAV-hSyn-mCherry (controls) or pAAV-hSyn-hM3D(Gq)-mCherry (TLS) and implanted with telemetric temperature probes. Mice were administered CNO water (0.01–0.04 mM) for 4 days, followed by 3 days of recovery over 12 weeks. Bodyweight was measured every 2 weeks.

Food intake was measured twice a week—upon CNO administration and removal—allowing us to capture food consumption while on and off CNO.

Tissue processing

Mice were anesthetized via inhalation of isoflurane and euthanized by cervical dislocation. Blood was collected via cardiac puncture followed by transcardial perfusion of 10 ml PBS to wash tissues. Tissues were removed and washed in PBS twice before being flash frozen in liquid nitrogen. Following collection, tissues were stored at -80 °C before further processing. For DNA extraction, DNeasy Blood & Tissue Kits were used (QIAGEN catalog number 69506). After extraction, DNA was stored at -20 °C until further processing. For RNA extraction, RNeasy Mini kits were used (QIAGEN catalog number 74104). After extraction, RNA was stored at -80 °C until further processing.

Methylation analysis

DNA samples were normalized to between 12.5 and 25 ng µl⁻¹ in 30 µl. DNA was bisulfite converted using the Zymo EZ DNA methylation kit (D5004). Bisulfite-converted DNA was run on the Illumina Horvath Mammalian Methylation 320K Chip, which combines the Illumina Infinium Mouse Methylation 285k array with the mammalian methylation array, resulting in interrogation of >285,000 cytosine–phosphate–guanine (CpG) sites specific to mice and 37,000 conserved mammalian loci⁴³. The SEnsible Step-wise Specific Analysis of DNA MEthylation BeadChips (SeSaMe) normalization method was used to estimate methylation levels (β values) for each CpG site.

Epigenetic clock analysis

Our epigenetic clocks are based on the HorvathMammalMethylChip320. The data were generated and analyzed by the nonprofit Epigenetic Clock Development Foundation as previously described^{20,21,23,43,44}. In our primary analysis (Fig. 2), we assessed the epigenetic ages of various mouse tissues by using DNA methylation clocks tailored for blood, liver, kidney, and cerebral cortex. These mouse methylation clocks were developed based on distinct training datasets as reported by ref. 44. We also used the universal pan-mammalian epigenetic clocks (UniversalClock 2 and 3), as described by ref. 23 and depicted in Extended Data Fig. 3. These pan-mammalian clocks leverage conserved cytosines to evaluate aging across mammalian species, highlighting epigenetic aging effects likely relevant to human aging. The R code of all of these epigenetic clocks can be found in the MammalMethylClock R package (1.0.0.)⁴⁵.

Differential methylation analysis

Differential methylation analysis was performed using the SeSaMe pipeline (v.1.16). First, the differentially methylated loci function was used to identify differentially methylated probes between control and TLS mice. The differentially methylated region (DMR) function was then used to align probes to the mouse genome (mm10) and find differentially methylated regions. The following thresholds for significance were used, an adjusted $P < 10^{-3}$ and $|\Delta\beta| > 0.05$.

GREAT analysis

Gene enrichment and top biological processes analysis were performed using the Genomic Regions Enrichment of Annotations Tool (GREAT) v.4.0.4. In brief, differentially methylated regions were identified as described above. Only genomic regions with an adjusted $P < 0.001$ and $|\Delta\beta| > 0.05$ were used for GREAT analysis with a basal plus extension of 5 kb proximal upstream, 1 kb proximal downstream, plus distal of up to 1 kb.

Bulk RNA-sequencing library preparation and sequencing

Libraries were prepared using the NEBNext Ultra II kit. In brief, 500 ng of RNA per sample underwent Poly(A) selection before fragmentation

and random priming followed by first- and second-strand complementary DNA synthesis. Following cDNA synthesis, NEBNext Multiplex Oligos for Illumina (E6440S) were ligated before PCR enrichment. All libraries were pooled to a final concentration of 1 nM and sequenced on a NovaSeq 6000.

Transcriptomic clock analysis

To assess the transcriptomic age (tAge) of liver, white adipose tissue, cortex, and kidney derived from control mice and mice subjected to TLS, we applied a mouse multi-tissue gene expression clock of relative lifespan-adjusted age based on previously identified signatures of aging and lifespan-regulating interventions^{46,47}. Genes with less than 5 reads in more than 87.5% of samples were filtered out, resulting in 17,695 expressed genes according to Entrez annotation. Filtered data were then passed to relative log expression normalization⁴⁸. Normalized gene expression profiles were log-transformed and scaled. The missing values corresponding to clock genes not detected in the data were imputed with the precalculated average values. Samples from control 4-month-old animals were used as reference groups for every tissue. Differences between average tAges across the groups were assessed with one-sample analysis of variance (ANOVA) and adjusted for multiple comparisons using Tukey's honestly significant difference (HSD).

Differential gene expression

The following command was used to align reads to the mm10 reference mouse genome using STAR v2.7.10:

```
for fq1 in '/bin/ls *R1_001.fastq.gz'
do
name = 'basename $fq1 | perl -pe "s/_R1_001.fastq.gz//"'
fq2 = 'basename $fq1 | perl -pe "s/R1_001.fastq.gz/R2_001.fastq.gz/"'
echo Processing $name...
# Slurm cluster call
# echo sbatch --partition=20 --job-name=STAR --mem=32 G
--wrap "STAR --genomeDir /nfs/genomes/mouse_mm10_dec_11_no_random/STAR/GRCm38.102.canonical_overhang_100
--sjdbScore 2 --runThreadN 8 --outSAMtype BAM SortedByCoordinate --readFilesCommand zcat --readFilesIn $fq1 $fq2
--outFileNamePrefix./STAR/$name."
sbatch --partition=20 --job-name=STAR --mem=32 G --wrap
"STAR --genomeDir /nfs/genomes/mouse_mm10_dec_11_no_random/STAR/GRCm38.102.canonical_overhang_100
--sjdbScore 2 --runThreadN 8 --outSAMtype BAM SortedByCoordinate --readFilesCommand zcat --readFilesIn $fq1 $fq2
--outFileNamePrefix./STAR/$name."
done
```

After alignment, data were processed through the DESeq2 pipeline. In brief, data were separated by tissue type and processed independently. DESeq() was run to normalize counts using contrast of treatment (TLS versus Con). DESeq results were transformed to variance-stabilized expression levels using the vst() function followed by log fold change shrinkage with the lfcShrink() function using apeglm. Data were visualized using the EnhancedVolcano() function with the following thresholds: $-\log_{10}(P) < 10^{-6}$ and $\log_2 \text{fold change} > 1$.

Clinical frailty index

Clinical frailty measurements were performed as previously described^{26,27}. In brief, a blinded investigator scored mice on 31 noninvasive measures using a simple scale: mice were given a 0 if they showed no deficit, a 0.5 if they showed a mild deficit, and a 1 if they showed a severe deficit. All frailty measurements were performed when mice were off CNO and had recovered to euthermia. All bodyweight and temperature calculations were excluded from downstream frailty score analyses given the confounding effects of TLS on T_b and bodyweight.

Clamping T_a

To blunt decreases in core T_b , mice cages were placed at a thermoneutral temperature (32 °C) in a Powers Scientific Incubator (IT54SD) for the duration of the experiment.

Caloric restriction

CR 32 °C mice and Stim + CR 32 °C mice were pair-fed to TLS mice 4 days a week and fed ad libitum 3 days a week to isolate the effects of caloric restriction during TLS. In brief, CR 32 °C mice, Stim + CR 32 °C mice, and Con 32 °C mice were singly housed at thermoneutral T_a (32 °C). We measured that while on CNO, TLS mice (1.17 ± 0.1 g) ate on average 35% of what Con 22 °C mice ate (3.31 ± 0.14 g). We found that, while on CNO, Stim 32 °C mice (2.30 ± 0.12 g) ate on average 70% of what Con 32 °C mice ate (3.25 ± 0.22 g). When pair-feeding CR 32 °C mice and Stim + CR 32 °C mice to TLS mice, we accounted for the difference in basal metabolic rates between mice housed at 32 °C versus 22 °C and thus fed mice 1 ± 0.1 g of food per day (roughly equivalent to 35% of the daily food intake of Con 32 °C mice). While on CNO, CR 32 °C mice and Stim + CR 32 °C were fed daily at the beginning of the dark cycle. While off CNO, CR 32 °C mice and Stim + CR 32 °C mice were fed ad libitum. Food intake of all mice was measured twice weekly, once at the beginning of CNO treatment and once at the end.

Statistics and reproducibility

Sample size was predetermined based on power analyses from previously reported epigenetic clocks²¹ and estimates based on effect size of hibernation on epigenetic age in other species²⁵. Pre-established criteria were used for data inclusion/exclusion. Mainly, in long-term epigenetic experiments, only animals from which we were able to extract sufficient blood for downstream processing were included at each measured time point. Each experiment was performed a single time with multiple animals (numbers indicated in manuscript). Data are displayed as individual points indicating the distribution of results throughout the manuscript. In independent experiments that overlapped in groups (that is, TLS mice in short-term and long-term experiments), the results were in agreement. Assignment of age- and gender-matched mice to different surgical and experimental groups was random. All epigenetic clock analyses were performed blinded to group. Frailty measurements were performed blinded to group. Data distribution was assumed to be normal, but this was not formally tested; all data are plotted as individual data points.

Reporting summary

Further information on research design is available in the Nature Portfolio Reporting Summary linked to this article.

Data availability

All raw and processed methylation data are deposited and available at Gene Expression Omnibus database (GEO) (GEO accession numbers [282499](#), [282659](#), [282661](#)). Raw and processed RNA-seq data are deposited and available at GEO (GEO accession number [GSE288355](#)). All additional source data are available in supplementary information files. If there are any additional data missing from repositories and/or supplemental information files, data are available from the corresponding author upon reasonable request. RNA-seq reads were aligned to the mm10 reference mouse genome using STAR v2.7.10. The mm10 reference genome is available at the National Center for Biotechnology Information RefSeq assembly (GCF 000001635.20).

Code availability

Analysis was performed in R (v.4.2.1), Python (v.3.8.5), and GraphPad Prism (v.10.2.3). Statistical analysis of the thermoregulatory system was performed as previously described with publicly available code^{10,15}. R code for all epigenetic clocks used can be found in the MammalMethylClock R package⁴³. Differential methylation analysis was performed

using the SeSaMe pipeline. Gene enrichment and biological processes analyses were performed using the Genomic Regions Enrichment of Annotations Tool (GREAT v.4.0.4). Transcriptomic clock analysis was performed as previously described^{44–46} by A. Tyshkovskiy using R package edgeR (v.4.2.0)⁴⁸. Differential gene expression was performed using DESeq2 (v.1.46). All custom code are available from the corresponding author upon reasonable request.

References

- Wilkinson, G. S. & Adams, D. M. Recurrent evolution of extreme longevity in bats. *Biol. Lett.* **15**, 20180860 (2019).
- Tan, C. L. & Knight, Z. A. Regulation of body temperature by the nervous system. *Neuron* **98**, 31–48 (2018).
- Morrison, S. F. & Nakamura, K. Central mechanisms for thermoregulation. *Annu. Rev. Physiol.* **81**, 285–308 (2019).
- Boulant, J. A. & Hardy, J. D. The effect of spinal and skin temperatures on the firing rate and thermosensitivity of preoptic neurones. *J. Physiol.* **240**, 639–660 (1974).
- Tan, C. L. et al. Warm-sensitive neurons that control body temperature. *Cell* **167**, 47–59.e15 (2016).
- Yu, S. et al. Glutamatergic preoptic area neurons that express leptin receptors drive temperature-dependent body weight homeostasis. *J. Neurosci.* **36**, 5034–5046 (2016).
- Wang, T. A. et al. Thermoregulation via temperature-dependent PGD(2) production in mouse preoptic area. *Neuron* **103**, 349 (2019).
- Hrvatin, S. et al. Neurons that regulate mouse torpor. *Nature* **583**, 115–121 (2020).
- Zhang, Z. et al. Estrogen-sensitive medial preoptic area neurons coordinate torpor in mice. *Nat. Commun.* **11**, 6378 (2020).
- Takahashi, T. M. et al. A discrete neuronal circuit induces a hibernation-like state in rodents. *Nature* **583**, 109–114 (2020).
- Yang, Y. et al. Induction of a torpor-like hypothermic and hypometabolic state in rodents by ultrasound. *Nat. Metab.* **5**, 789–803 (2023).
- Geiser, F. Metabolic rate and body temperature reduction during hibernation and daily torpor. *Annu. Rev. Physiol.* **66**, 239–274 (2004).
- Heller, H. C. The physiology of hibernation. *Science* **220**, 599–600 (1983).
- Sunagawa, G. A. & Takahashi, M. Hypometabolism during daily torpor in mice is dominated by reduction in the sensitivity of the thermoregulatory system. *Sci. Rep.* **6**, 37011 (2016).
- Swoap, S. J. & Gutilla, M. J. Cardiovascular changes during daily torpor in the laboratory mouse. *Am. J. Physiol. Regul. Integr. Comp. Physiol.* **297**, R769–R774 (2009).
- Hitrec, T. et al. Neural control of fasting-induced torpor in mice. *Sci. Rep.* **9**, 15462 (2019).
- Florant, G. L. & Heller, H. C. CNS regulation of body temperature in euthermic and hibernating marmots (*Marmota flaviventris*). *Am. J. Physiol.* **232**, R203–R208 (1977).
- Heller, H. C. & Colliver, G. W. CNS regulation of body temperature during hibernation. *Am. J. Physiol.* **227**, 583–589 (1974).
- Heller, H. C., Colliver, G. W. & Anand, P. CNS regulation of body temperature in euthermic hibernators. *Am. J. Physiol.* **227**, 576–582 (1974).
- Horvath, S. & Raj, K. DNA methylation-based biomarkers and the epigenetic clock theory of ageing. *Nat. Rev. Genet.* **19**, 371–384 (2018).
- Thompson, M. J. et al. A multi-tissue full lifespan epigenetic clock for mice. *Aging* **10**, 2832–2854 (2018).
- Horvath, S. DNA methylation age of human tissues and cell types. *Genome Biol.* **14**, R115 (2013).
- Lu, A. T. et al. Universal DNA methylation age across mammalian tissues. *Nat. Aging* **3**, 1144–1166 (2023).
- Sullivan, I. R., Adams, D. M., Greville, L. J. S., Faure, P. A. & Wilkinson, G. S. Big brown bats experience slower epigenetic ageing during hibernation. *Proc. Biol. Sci.* **289**, 20220635 (2022).
- Pinho, G. M. et al. Hibernation slows epigenetic ageing in yellow-bellied marmots. *Nat. Ecol. Evol.* **6**, 418–426 (2022).
- Schultz, M. B. et al. Age and life expectancy clocks based on machine learning analysis of mouse frailty. *Nat. Commun.* **11**, 4618 (2020).
- Whitehead, J. C. et al. A clinical frailty index in aging mice: comparisons with frailty index data in humans. *J Gerontol. A* **69**, 621–632 (2014).
- Conti, B. et al. Transgenic mice with a reduced core body temperature have an increased life span. *Science* **314**, 825–828 (2006).
- Zhao, Z. et al. Body temperature is a more important modulator of lifespan than metabolic rate in two small mammals. *Nat. Metab.* **4**, 320–326 (2022).
- Pearl, R. *The Rate of Living, Being an Account of Some Experimental Studies on the Biology of Life Duration* (A.A. Knopf, 1928).
- Rubner, M. *Das Problem des Lebensdauers und seiner Beziehungen zum Wachstum und Ernährung* (Oldenbourg, 1908).
- Kleiber, M. Body size and metabolic rate. *Physiol. Rev.* **27**, 511–541 (1947).
- McCay, C. M., Crowell, M. F. & Maynard, L. A. The effect of retarded growth upon the length of life span and upon the ultimate body size. *Nutrition* **5**, 155–171 (1935).
- Mitchell, S. E. et al. The effects of graded levels of calorie restriction: III. Impact of short term calorie and protein restriction on mean daily body temperature and torpor use in the C57BL/6 mouse. *Oncotarget* **6**, 18314–18337 (2015).
- Lyman, C. P., O'Brien, R. C., Greene, G. C. & Papafrangos, E. D. Hibernation and longevity in the Turkish hamster *Mesocricetus brandti*. *Science* **212**, 668–670 (1981).
- Koizumi, A. et al. A tumor preventive effect of dietary restriction is antagonized by a high housing temperature through deprivation of torpor. *Mech. Ageing Dev.* **92**, 67–82 (1996).
- Acosta-Rodriguez, V. et al. Circadian alignment of early onset caloric restriction promotes longevity in male C57BL/6J mice. *Science* **376**, 1192–1202 (2022).
- Higgins-Chen, A. T., Boks, M. P., Vinkers, C. H., Kahn, R. S. & Levine, M. E. Schizophrenia and epigenetic aging biomarkers: increased mortality, reduced cancer risk, and unique clozapine effects. *Biol. Psychiatry* **88**, 224–235 (2020).
- Manvich, D. F. et al. The DREADD agonist clozapine N-oxide (CNO) is reverse-metabolized to clozapine and produces clozapine-like interoceptive stimulus effects in rats and mice. *Sci. Rep.* **8**, 3840 (2018).
- Perez-Aldana, B. E. et al. Clozapine long-term treatment might reduce epigenetic age through hypomethylation of longevity regulatory pathways genes. *Front. Psychiatry* **13**, 870656 (2022).
- Rao, P. N. & Engelberg, J. Hela cells: effects of temperature on the life cycle. *Science* **148**, 1092–1094 (1965).
- Rieder, C. L. & Cole, R. W. Cold-shock and the mammalian cell cycle. *Cell Cycle* **1**, 169–175 (2002).
- Arneson, A. et al. A mammalian methylation array for profiling methylation levels at conserved sequences. *Nat. Commun.* **13**, 783 (2022).
- Mozhui, K. et al. Genetic loci and metabolic states associated with murine epigenetic aging. *Elife* **11**, e75244 (2022).
- Zoller, J. A. & Horvath, S. MammalMethylClock R package: software for DNA methylation-based epigenetic clocks in mammals. *Bioinformatics* **40**, btae280 (2024).
- Tyshkovskiy, A. et al. Identification and application of gene expression signatures associated with lifespan extension. *Cell Metab.* **30**, 573–593.e578 (2019).

47. Tyshkovskiy, A. et al. Distinct longevity mechanisms across and within species and their association with aging. *Cell* **186**, 2929–2949.e2920 (2023).
48. Robinson, M. D., McCarthy, D. J. & Smyth, G. K. edgeR: a bioconductor package for differential expression analysis of digital gene expression data. *Bioinformatics* **26**, 139–140 (2010).

Acknowledgements

We thank the University of California, Los Angeles, Neuroscience Genomics Core for processing DNA samples for methylation analysis. We thank G. Bell from the Bioinformatics and Research Computing group at the Whitehead Institute for help processing RNA sequencing (RNA-seq) data. We thank M. E. Greenberg for providing feedback on the study. We thank the Clock Foundation for applying epigenetic clocks to generate DNAmAge estimates. We thank Beth Israel Deaconess Medical Center Metabolic Core for performing metabolic experiments. We thank the Sinclair lab for teaching us how to perform frailty index measurements. This project was supported by Longevity Impetus Grants from Norn Group to S. Hrvatin and V.N.G, the National Institute of Health grant 1DP2DK136123-01 to S. Hrvatin, and the National Institute of Aging grant AG067782 to V.N.G.

Author contributions

L.J. and S. Hrvatin conceived and designed the study. L.J. designed, performed and analyzed experiments. A.L.-P. designed and performed experiments. A.T. performed transcriptomic clock analyses (tAge). M.A. designed and performed experiments. J.R., E.R., A.M., S.S. and H.Y. contributed to experiments. R.T.B. and S. Horvath applied epigenetic clocks to methylation data to generate DNAmAge estimates. V.N.G., V.G.S., and E.C.G. advised on the study. L.J., S. Hrvatin and E.C.G. wrote the paper. L.J., E.C.G. and S. Hrvatin obtained funding for the research. All authors approved and reviewed the paper.

Competing interests

S. Horvath and R.T.B. are founders of the non-profit Epigenetic Clock Development Foundation, which licenses several patents from UC Regents including a patent on the mammalian methylation array platform. These patents list S. Horvath as inventor. V.G.S. serves as an advisor to and/or has equity in Branch Biosciences, Ensoma, and Cellarity, all unrelated to this work. S. Hrvatin is an advisor to

Apertura LLC, unrelated to this work. The other authors declare no competing interests.

Additional information

Extended data is available for this paper at
<https://doi.org/10.1038/s43587-025-00830-4>.

Supplementary information The online version contains supplementary material available at
<https://doi.org/10.1038/s43587-025-00830-4>.

Correspondence and requests for materials should be addressed to Sinisa Hrvatin.

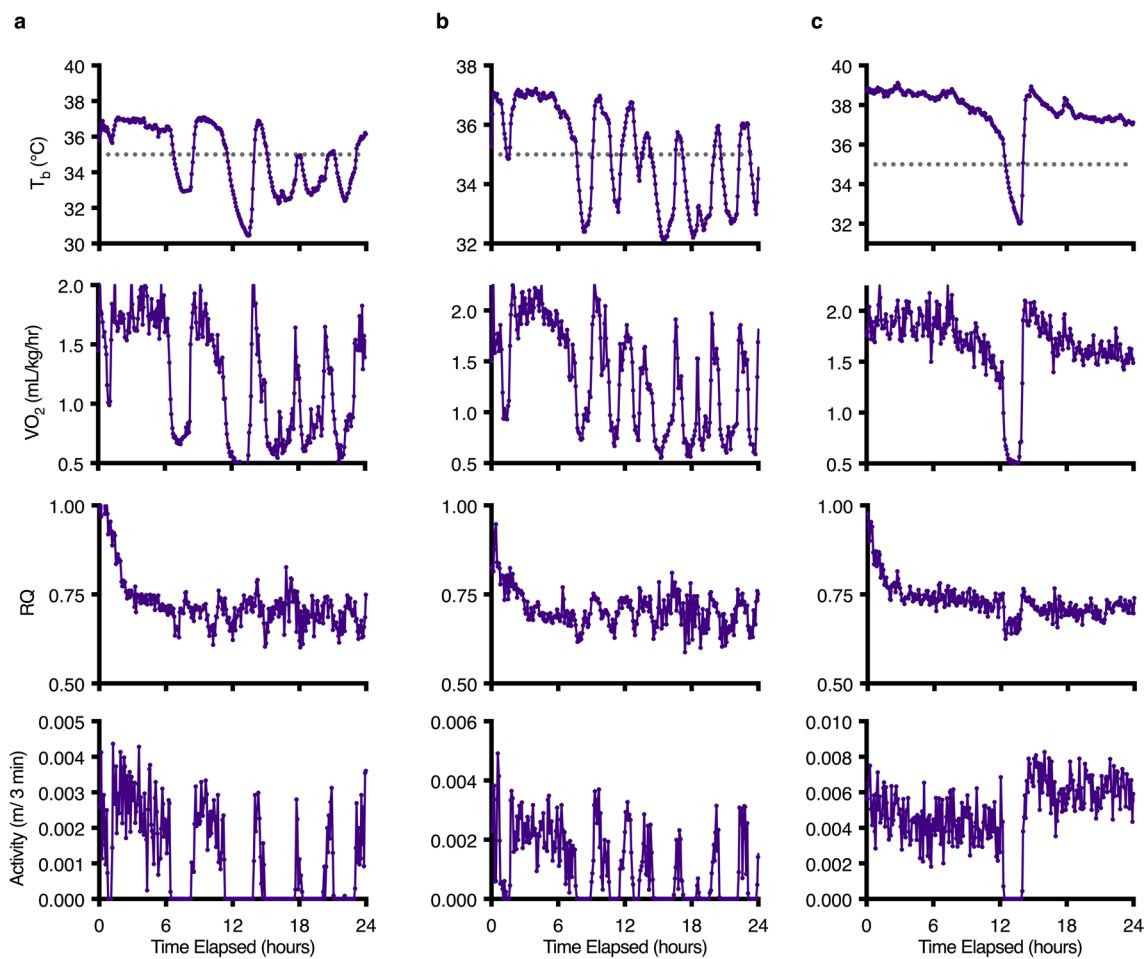
Peer review information *Nature Aging* thanks Andrzej Bartke, Matteo Cerri, Khyobeni Mozhui and the other, anonymous, reviewer(s) for their contribution to the peer review of this work.

Reprints and permissions information is available at
www.nature.com/reprints.

Publisher's note Springer Nature remains neutral with regard to jurisdictional claims in published maps and institutional affiliations.

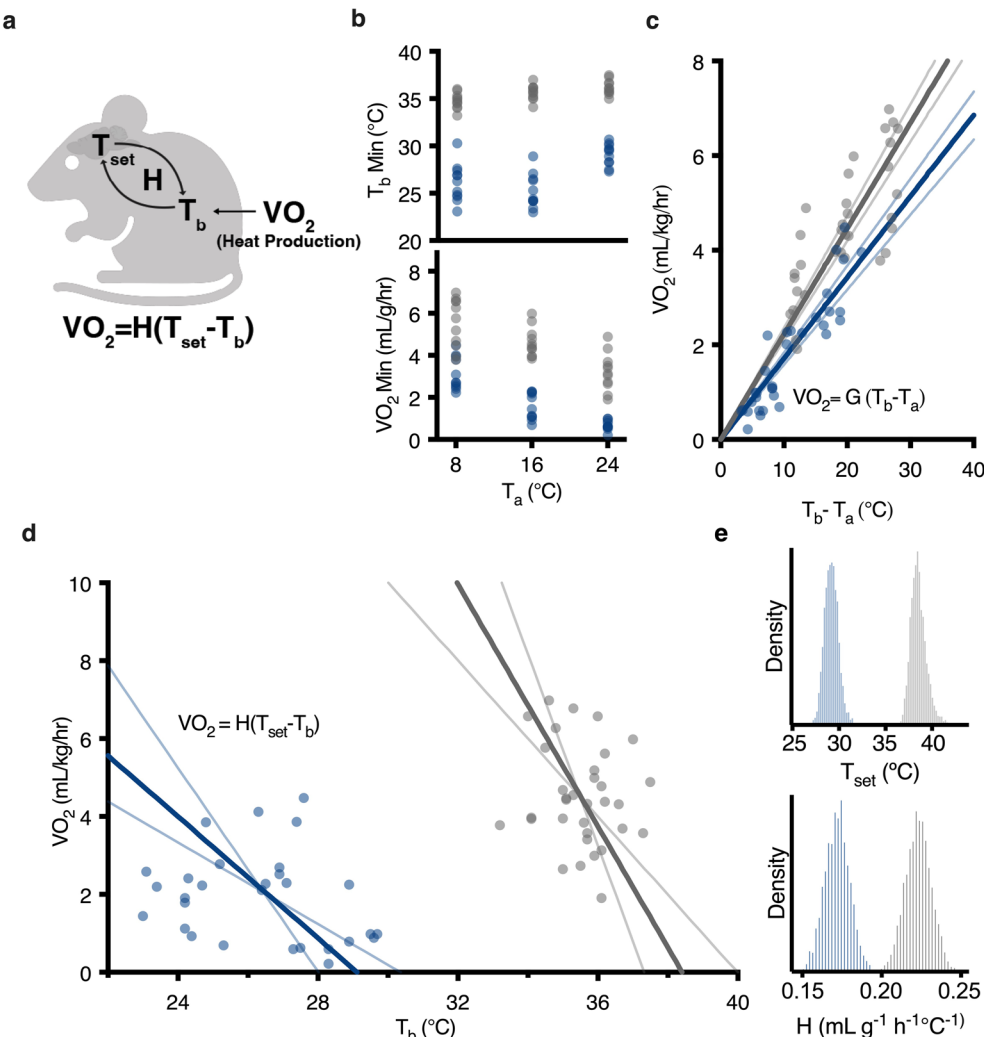
Open Access This article is licensed under a Creative Commons Attribution-NonCommercial-NoDerivatives 4.0 International License, which permits any non-commercial use, sharing, distribution and reproduction in any medium or format, as long as you give appropriate credit to the original author(s) and the source, provide a link to the Creative Commons licence, and indicate if you modified the licensed material. You do not have permission under this licence to share adapted material derived from this article or parts of it. The images or other third party material in this article are included in the article's Creative Commons licence, unless indicated otherwise in a credit line to the material. If material is not included in the article's Creative Commons licence and your intended use is not permitted by statutory regulation or exceeds the permitted use, you will need to obtain permission directly from the copyright holder. To view a copy of this licence, visit <http://creativecommons.org/licenses/by-nc-nd/4.0/>.

© The Author(s) 2025



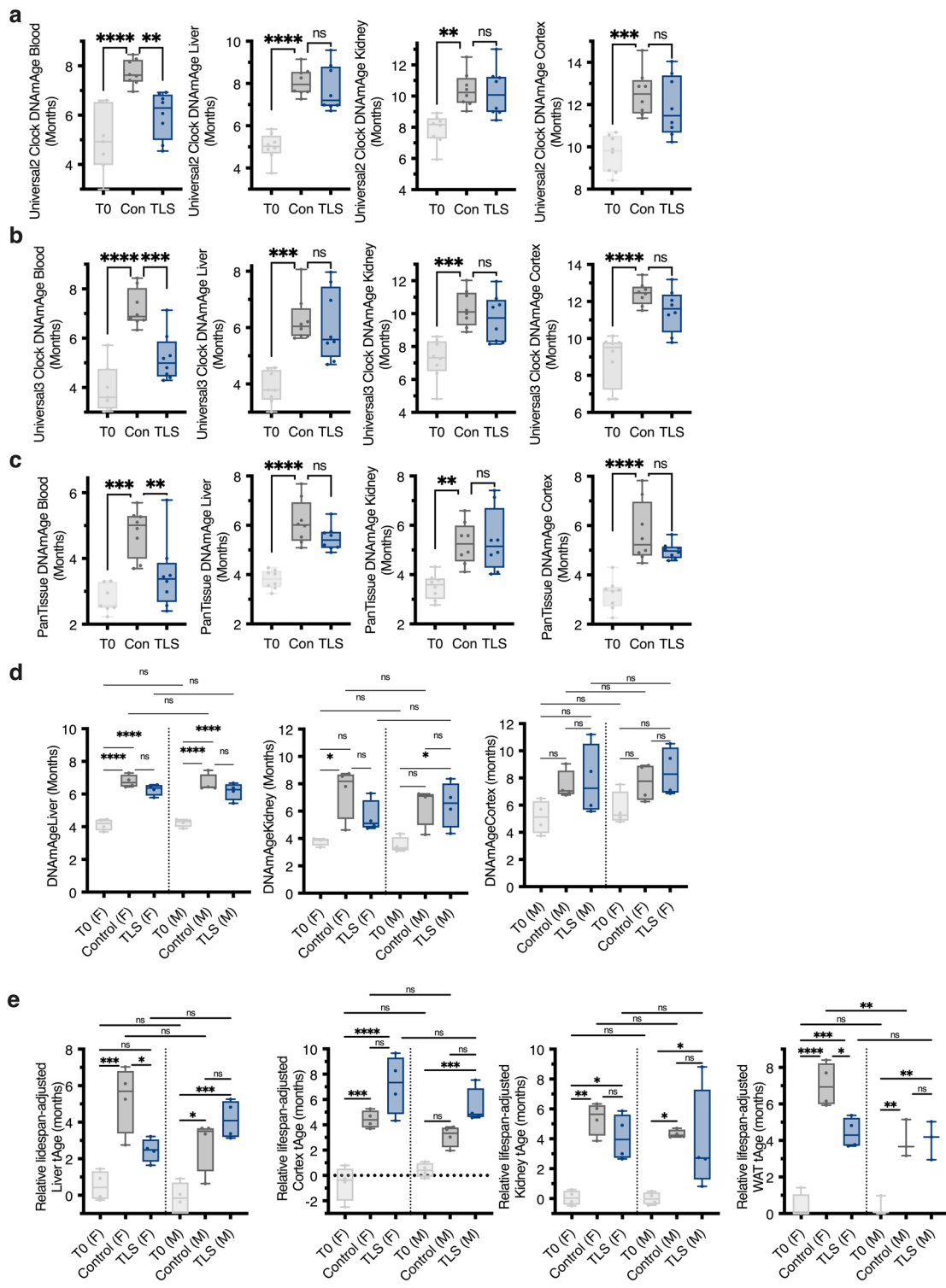
Extended Data Fig. 1 | Metabolic characterization of natural fasting-induced daily torpor bouts. a-c, T_b , VO_2 , RQ, and activity as measured by the Prometheon Metabolic System in 3 representative individual mice over a 24-hour fasting interval (food was removed at time 0). 6/8 mice underwent natural fasting-

induced daily torpor bouts during the fasting interval as defined by $T_b < 35^\circ\text{C}$ and lack of arousal (threshold T_b for torpor entry marked by dotted grey line on T_b graph).



Extended Data Fig. 2 | The thermoregulatory system during TLS. **a**, Schematic of the thermoregulatory model. **b**, Minimum T_b and VO_2 across ambient temperatures (8, 16, 24°C) at baseline (grey) and during TLS (blue) ($n = 11$). **c**, The relationship between VO_2 and $T_b - T_a$. The slope of the curve denotes the median value of G , the heat conductance, at baseline (grey) ($0.233 \text{ mL g}^{-1} \text{ h}^{-1} \text{ }^{\circ}\text{C}^{-1}$) and during TLS (blue) ($0.172 \text{ mL g}^{-1} \text{ h}^{-1} \text{ }^{\circ}\text{C}^{-1}$), thin lines denote the 89% highest posterior density interval (HPDI) of G at baseline [$0.210, 0.236$] $\text{mL g}^{-1} \text{ h}^{-1} \text{ }^{\circ}\text{C}^{-1}$ and during TLS [$0.159, 0.184$] $\text{mL g}^{-1} \text{ h}^{-1} \text{ }^{\circ}\text{C}^{-1}$, and dots represent data. **d**,

Relationship between T_b and VO_2 across varying T_a . The negative slope denotes the median value of H at baseline (grey) ($1.555 \text{ g}^{-1} \text{ h}^{-1} \text{ }^{\circ}\text{C}^{-1}$) and during TLS (blue) ($0.780 \text{ g}^{-1} \text{ h}^{-1} \text{ }^{\circ}\text{C}^{-1}$). The X-intercept, where $VO_2 = 0$, represents the median theoretical set point temperature (T_{set}) at baseline (38.414°C) and during TLS (29.13°C), thin lines represent the 89% HPDI of both H [$1.00, 2.46$] $\text{g}^{-1} \text{ h}^{-1} \text{ }^{\circ}\text{C}^{-1}$ at baseline and [$0.52, 1.31$] $\text{g}^{-1} \text{ h}^{-1} \text{ }^{\circ}\text{C}^{-1}$ during TLS and T_{set} [$37.323, 40.0$] $^\circ\text{C}$ at baseline and 29.13 [$28.02, 30.36$] $^\circ\text{C}$ during TLS, dots represent data. **e**, Distribution of estimated T_{set} and H both at baseline (grey) and during TLS (blue).

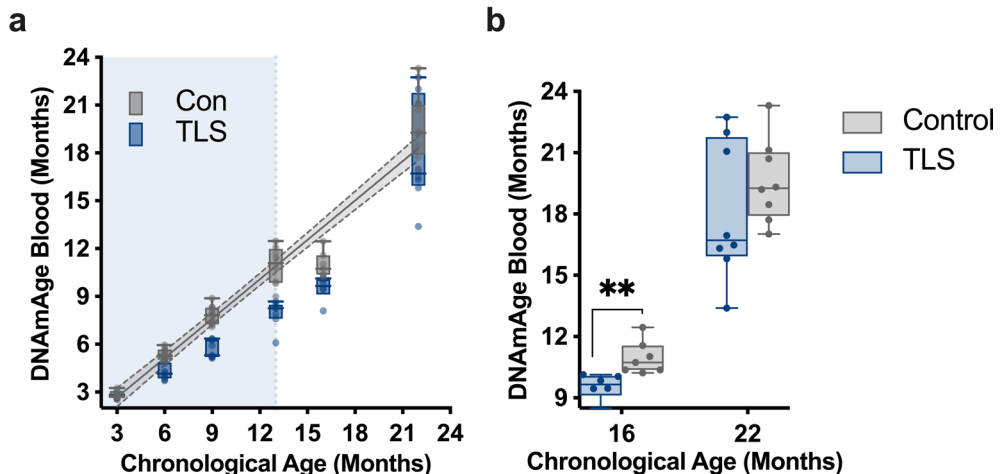


Extended Data Fig. 3 | See next page for caption.

Extended Data Fig. 3 | Additional epigenetic and transcriptomic clock analyses.

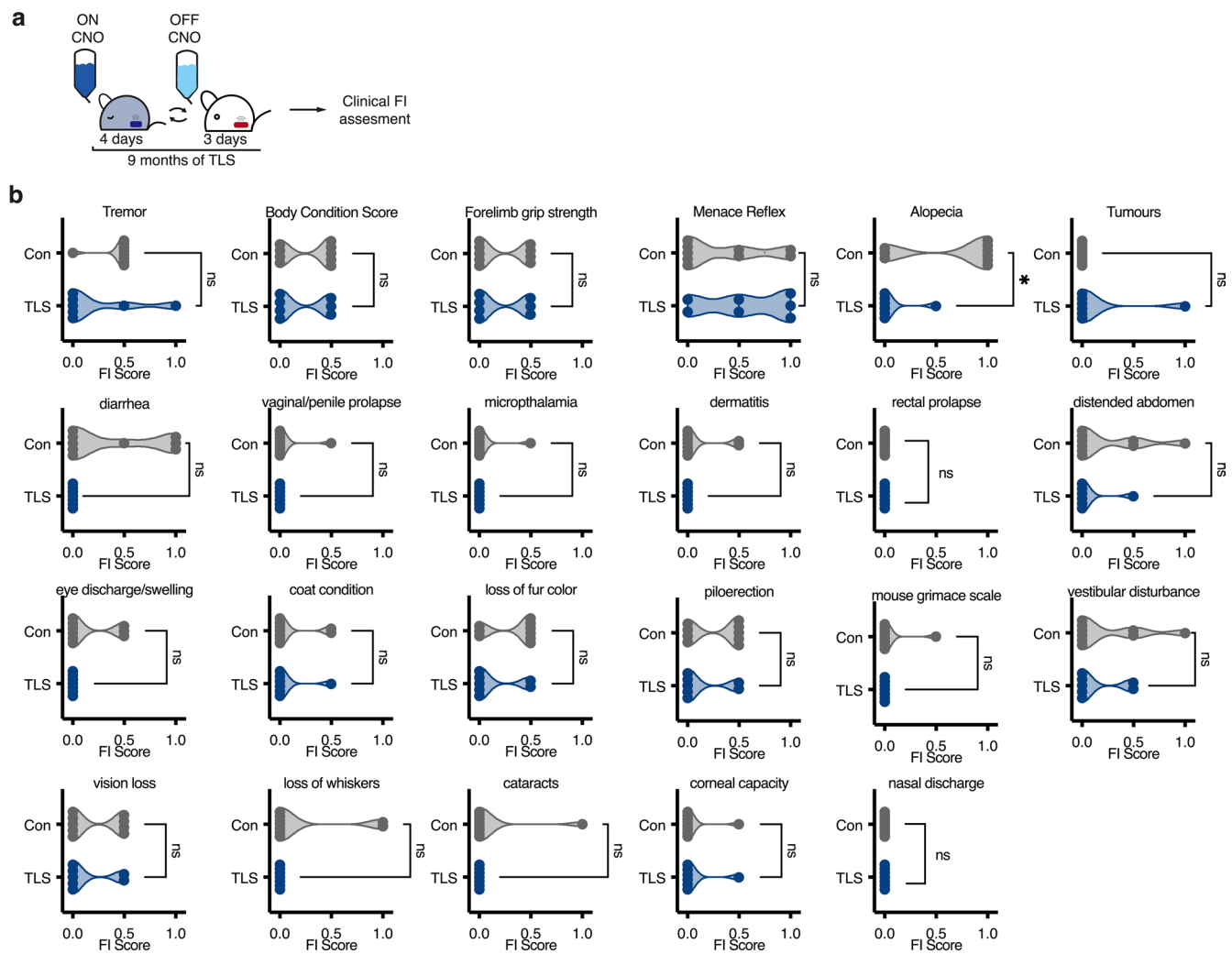
a, DNAmAge across tissues as calculated using the Universal2 Epigenetic Clock. Data reported as mean \pm SEM. Significance determined by one-way ANOVA adjusted for multiple comparisons by Tukey's HSD. In the blood, TLS mice (6.01 ± 0.33) had significantly lower DNAmAge than control mice ($n = 8$) (7.34 ± 0.18) ($**P = 0.0015$). In the liver, kidney, and cortex, TLS mice (liver = 7.76 ± 0.39 , kidney = 10.25 ± 0.56 , cortex = 11.92 ± 0.51) had comparable DNAmAge to control mice (liver = 8.08 ± 0.23 , kidney = 10.40 ± 0.39 , cortex = 12.54 ± 0.38) (liver = ns, $P = 0.7240$, kidney = ns, $P = 0.9705$, cortex = ns, $P = 0.5352$). **b**, DNAmAge across tissues as calculated using the Universal3 Epigenetic Clock. Data reported as mean \pm SEM. Significance determined by one-way ANOVA adjusted for multiple comparisons by Tukey's HSD. In the blood, TLS mice (5.22 ± 0.34) had significantly lower DNAmAge than control mice (7.21 ± 0.27) ($***P = 0.0008$). In the liver, kidney, and cortex, TLS mice (liver = 6.08 ± 0.45 , kidney = 9.71 ± 0.51 , cortex = 11.50 ± 0.41) had equivalent DNAmAge to control mice (liver = 6.28 ± 0.29 , kidney = 10.31 ± 0.39 , cortex = 12.41 ± 0.22) (liver = ns, $P = 0.7240$, kidney = ns, $P = 0.6152$, cortex = ns, $P = 0.2434$). **c**, DNAmAge across tissues as calculated using the PanTissue Epigenetic Clock. Data reported as mean \pm SEM. Significance determined by one-way ANOVA adjusted for multiple comparisons by Tukey's HSD. In the blood, TLS mice (3.5 ± 0.37) had significantly lower DNAmAge than control mice (4.80 ± 0.26) ($**P = 0.0099$). In the liver, kidney, and cortex, TLS mice (liver = 5.478 ± 0.18 , kidney = 5.40 ± 0.45 , cortex = 4.98 ± 0.12) had equivalent DNAmAge to control mice (liver = 6.13 ± 0.32 , kidney = 5.27 ± 0.30 , cortex = 5.72 ± 0.44) (liver = ns, $P = 0.1484$, kidney = ns, $P = 0.959$, cortex = ns, $P = 0.1997$). **d**, Tissue-specific epigenetic clock analyses across tissues and sexes. All data plotted as box plots indicating median, upper and lower quartiles, and whiskers extending to min and max values. Data reported as mean. Significance determined by one-way ANOVA adjusted for multiple comparisons by Tukey's HSD. In the liver, there were significant differences between T0 and control mice in both males (T0 M = 4.244 , M Control = 6.666 , $****P < 0.0001$) and females (T0 F = 4.143 , Control F = 6.788 , $****P < 0.0001$). There were significant differences between T0 and TLS mice in both males (T0 M = 4.224 , TLS M = 6.169 , $****P < 0.0001$) and females (T0 F = 4.143 , TLS F = 6.283 , $****P < 0.0001$). There were no significant differences between Control and TLS mice in both males (Control M = 6.666 , TLS M = 6.169 , ns, $P = 0.549$) and females (Control F = 6.788 , TLS F = 6.283 , ns, $P = 0.531$). Across sexes, there were no significant difference between T0 M and T0 F (ns, $P = 0.9990$), between Control M and Control F (ns, $P = 0.9981$), or between TLS M and TLS F (ns, $P = 0.9986$). In the cortex, we found no significant differences between any groups, suggesting the cortex tissue-specific clock lacked the necessary resolution. In the kidney, we found significant differences between T0 F (3.783) and Control F (7.438) ($*P = 0.010$); however, we did not find significance between T0 M (3.518) and Control M (6.444) (ns, $P = 0.0519$). We found a significant difference between T0 M and TLS M (6.482) ($*P = 0.0478$), however we found no significant difference between T0 F and TLS F (5.575) (ns, $P = 0.4139$). We found no significant differences between control females and TLS females (ns, $P = 0.3737$) or between control males and TLS males (ns, $P > 0.9999$). Across sexes, there were no significant difference between T0 M and T0 F (ns, $P = 0.9997$), between Control M and Control F (ns, $P = 0.8855$), or between TLS M and TLS F (ns, $P = 0.9187$). In the cortex there

were no significant differences between T0 and control mice in both males (T0 M = 5.129 , M Control = 7.475 , ns, $P = 0.3653$) and females (T0 F = 5.713 , Control F = 7.690 , ns, $P = 0.5434$). There were no significant differences between T0 and TLS mice in both males (TLS M = 7.813 , ns, $P = 0.2365$) and females (TLS F = 8.490 , ns, $P = 0.2075$). There were no significant differences between Control and TLS mice in both males (ns, $P = 0.3653$) and females (ns, $P = 0.9806$). Across sexes, there were no significant difference between T0 M and T0 F (ns, $P = 0.9953$), between Control M and Control F (ns, $P > 0.9999$), or between TLS M and TLS F (ns, $P = 0.9907$). **e**, Transcriptomic clock analysis across tissues. Data reported as mean. Significance determined by one-way ANOVA adjusted for multiple comparisons by Tukey's HSD. In the liver, there were significant differences between T0 and control mice in females (F) and males (M) (FT0 = 0.52 , F control = 5.29 , $***P = 0.0003$; M T0 = -0.24 , M control = 2.835 , $*P = 0.022$). There were significant differences between control and TLS mice in females (F control = 5.29 , F TLS = 2.46 , $*P = 0.039$), but not males (M control = 2.835 , M TLS = 4.15 , ns, $P = 0.649$). We found a significant difference between M T0 (- 0.2357) and M TLS (4.147), $***P = 0.0009$; however, this comparison was not significant in female mice (F T0 = 0.5166 , F TLS = 2.463 , ns, $P = 0.254$). Across sexes there were no significant differences between male and female T0 (ns, $P = 0.9467$), control (ns, $P = 0.090$), or TLS mice (ns, $P = 0.396$). In the cortex there were significant differences between T0 and control mice in females (FT0 = -0.60 , F control = 4.44 , $***P = 0.0002$) but not in males (M T0 = 0.43 , M control = 3.12 , ns, $P = 0.1473$). We found no significant differences between control and TLS mice in females (F control = 4.44 , F TLS = 7.17 , ns, $P = 0.1376$), or in males (M control = 3.12 , M TLS = 5.45 , ns, $P = 0.3055$). We found significant differences between T0 and TLS mice in both males ($***P = 0.0007$) and females ($****P < 0.0001$). Across sexes, there were no significant differences between male and female T0 (ns, $P = 0.9942$), control (ns, $P = 0.9476$), and TLS mice (ns, $P = 0.7365$). In the kidney, there were significant differences between T0 and control mice in both females (FT0 = 0.05 , F control = 5.37 , $**P = 0.0027$) and males (M T0 = 0.01 , M control = 4.33 , $*P = 0.0166$). There were no significant differences between control and TLS mice in females or males (F control = 5.37 , F TLS = 4.11 , ns, $P = 0.8792$; M control = 4.33 , M TLS = 3.76 , ns, $P = 0.9960$). We found significant differences between T0 and TLS mice in both males ($*P = 0.045$) and females ($*P = 0.0269$). Across sexes there were no significant differences between male and female T0 (ns, $P > 0.9999$), control (ns, $P = 0.9426$), and TLS mice (ns, $P = 0.9996$). In the WAT, there were significant differences between T0 and control mice in both females and males (FT0 = 0.17 , F control = 7.05 , $***P < 0.0001$) (M T0 = 0.22 , M control = 4.00 , $**P = 0.0025$). There were significant differences between control and TLS mice in females (F control = 7.05 , F TLS = 4.42 , $*P = 0.0153$), but not in males (M control = 4.00 , M TLS = 4.06 , ns, $P > 0.9999$). There were significant differences between T0 and TLS mice in both males ($**P = 0.0022$) and females ($***P = 0.0002$). Across sexes we found significant differences between F control and M control ($**P = 0.0009$). We found no significant differences between male and female T0 (ns, $P > 0.9999$) and TLS mice (ns, $P = 0.9959$). All data plotted as box plots indicating median, upper and lower quartiles, and whiskers extending to min and max values. Significance determined by one-way ANOVA adjusted for multiple comparisons by Tukey's HSD.



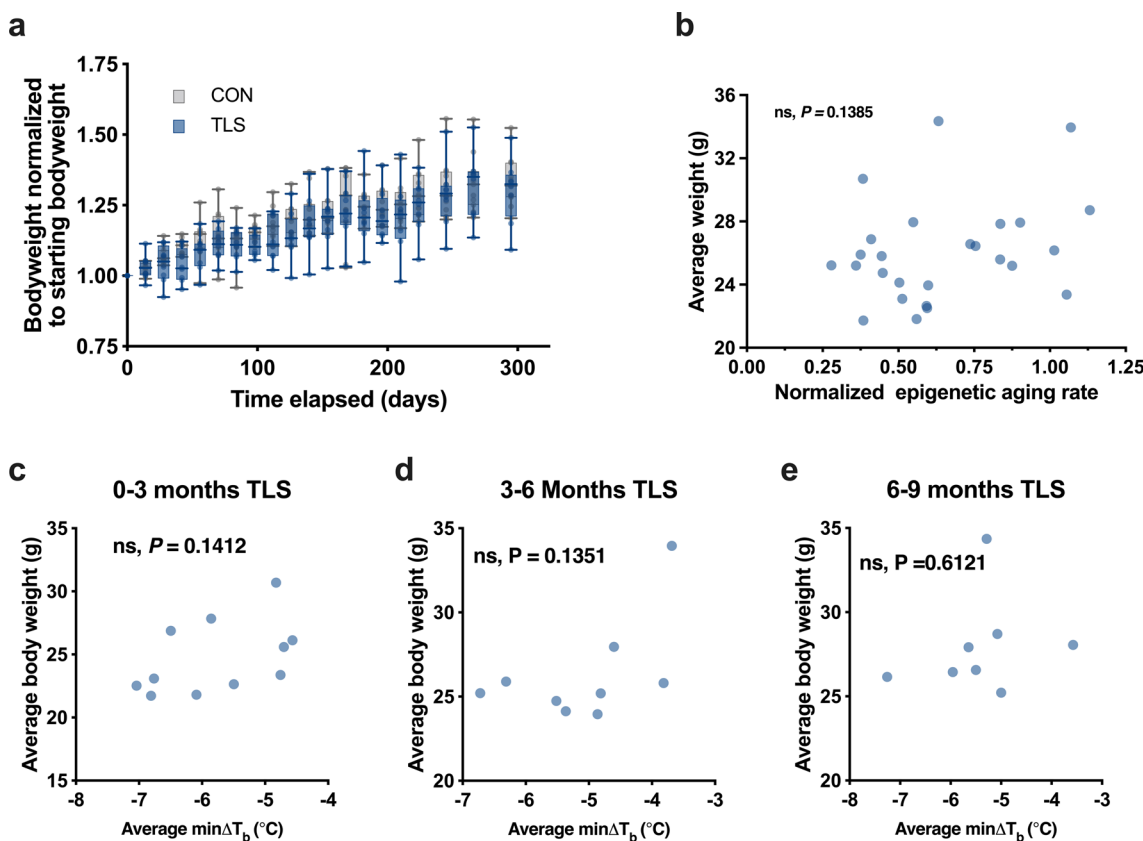
Extended Data Fig. 4 | Sustained effects of TLS on epigenetic age. **a**, DNAmAge blood of control (mice stereotactically injected in the avMLPA with AAV-hSyn-hM3D(Gq)-mCherry and administered drinking water without CNO) and TLS mice over the course of the experiment. Blue shading denotes CNO treatment. Data plotted as box plots (25th to 75th percentile) with whiskers from min-to-max with line at median. A standard curve ($DF = 54, R^2 = 0.934$) was interpolated across all timepoints in control mice to assess the measurements taken after 3 months of water. At 16 months of chronological age, the standard curve approximates that the blood DNAmAge of control mice would be 13.37 with 95% CI ± 0.494 . This value is higher than the observed value of 10.96 ± 0.305 ($n = 7$). Thus, while 3 months

post CNO cessation there is a smaller difference in epigenetic age between TLS and control mice, there is no evidence for an immediate acceleration of aging in TLS mice ($n = 6$) after cessation of CNO, rather this effect appears to reflect a possibly inaccurate measurement taken from control mice at 3 months post CNO cessation. **b**, Examining blood DNAmAge from 9 months after cessation of TLS indicates that while TLS mice ($n = 8$) still had an average blood DNAmAge (18.1 ± 1.19) - 1.5 months younger than control mice ($n = 8$) (19.87 ± 0.72) this difference did not reach significance as determined by unpaired two-tailed T-test ($ns, P = 0.297$). Data plotted as box plots (25th to 75th percentile) with whiskers from min-to-max with line at median.



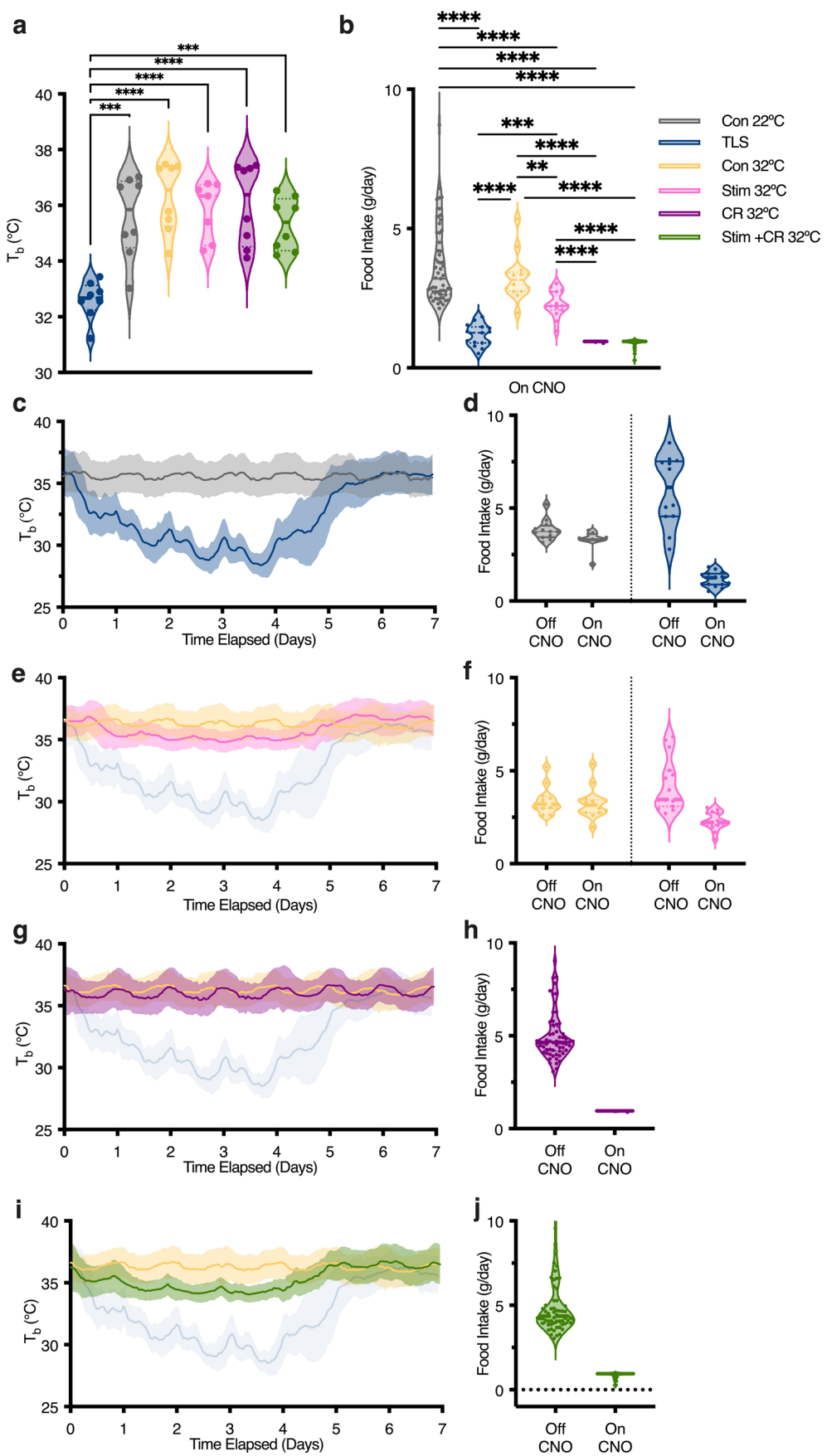
Extended Data Fig. 5 | Clinical Frailty Index measurements. **a**, Schematic of TLS treatment and clinical FI assessment. **b**, Frailty scores across the remaining 23 individual frailty index measurements of TLS and control mice (mice stereotactically injected in the avMLPA with AAV-hSyn-hM3D(Gq)-mCherry

and administered drinking water without CNO) after 9 months of TLS. TLS mice ($n=7$) (0.07 ± 0.0) scored significantly lower than control mice ($n=9$) (0.67 ± 0.0) on measurement of alopecia as determined by unpaired two-sided T-test ($*P=0.01$). Data reported as mean \pm SEM.



Extended Data Fig. 6 | Bodyweight and ΔT_b (°C) Analysis. **a**, Longitudinal measurements of bodyweight over 9 months. Control mice (mice stereotactically injected in the avMLPA with AAV-hSyn-hM3D(Gq)-mCherry and administered drinking water without CNO, grey) and TLS mice (blue) had similar bodyweights over the course of the experiment (TLS $n = 8$, Con $n = 11$). Using simple linear regression, we found that there was no significant difference in normalized bodyweight between TLS and control groups over the course of the longest study we performed (ns, $F = 0.0467$, DFn = 1, Dfd = 376, $P = 0.8290$). Data plotted as box plots (25th to 75th percentile) with whiskers from min-to-max with line at median. **b**, Average weight (g) plotted against the normalized epigenetic

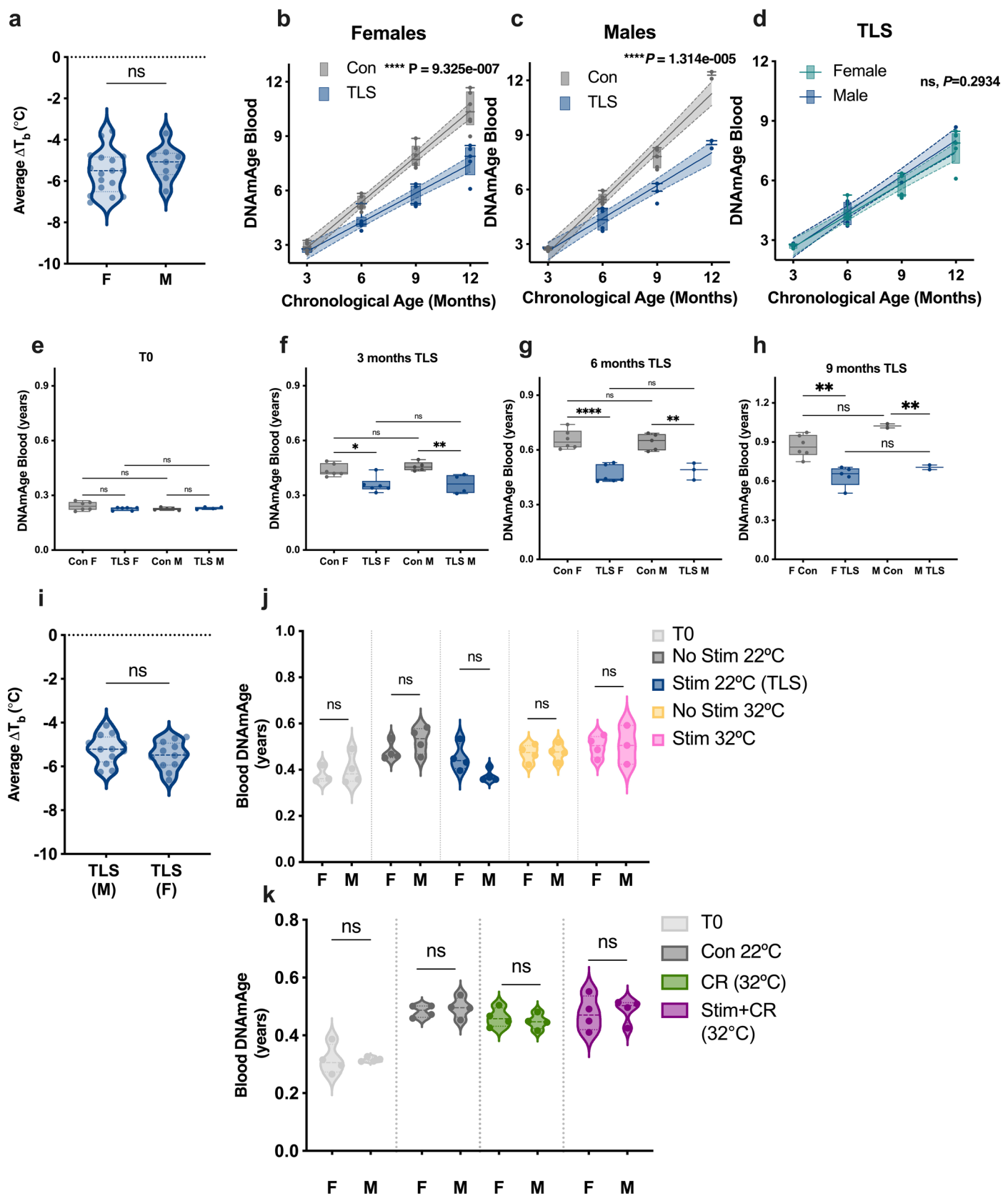
aging rate of individual TLS mice over the course of 9 months. We found no significant correlation between bodyweight and the rate of epigenetic aging as determined by Pearson correlation two-tailed test ($R^2 = 0.08914$, ns, $P = 0.1385$). **c-e**, To test whether average bodyweight correlates with decrease in core body temperature in TLS mice across any time points using Pearson two-tailed correlation tests (**c**, $R^2 = 0.2243$, ns, $P = 0.1412$, **d**, $R^2 = 0.2895$, ns, $P = 0.1351$, **e**, $R^2 = 0.04548$, ns, $P = 0.6121$).



Extended Data Fig. 7 | See next page for caption.

Extended Data Fig. 7 | Food intake and T_b in TLS, Con 22°C, Con 32°C, Stim 32°C, CR 32°C, and Stim + CR 32°C mice. **a.**, Average T_b of individual mice across all groups over 3 months. Significance determined by one-way ANOVA adjusted for multiple comparisons by Tukey's HSD Data reported as mean. TLS mice had significantly lower average T_b (32.6) than Con 32°C mice (36.28) (**** $P < 0.0001$), Stim + CR 32°C mice (35.33) (** $P = 0.0005$), CR 32°C mice (36.04) (**** $P < 0.0001$), Stim 32°C mice (35.83) (**** $P < 0.0001$), Con 22°C mice (35.58) (** $P = 0.0001$). There were no significant differences between Con 32°C and Stim + CR 32°C mice (ns, $P = 0.5964$), between Con 32°C mice and CR 32°C mice (ns, $P = 0.9983$), between Con 32°C and Stim 32°C mice (ns, $P = 0.9737$), between Con 32°C and Con 22°C mice (ns, $P = 0.8410$), between Stim + CR 32°C and CR 32°C mice (ns, $P = 0.8357$), between Stim + CR 32°C and Stim 32°C mice (ns, $P = 0.9654$), between Stim + CR 32°C and Con 22°C mice (ns, $P = 0.9981$), between CR 32°C and Stim 32°C mice (ns, $P = 0.9992$), between CR 32°C and Con 22°C mice (ns, $P = 0.9707$), and between Stim 32°C and Con 22°C mice (ns, $P = 0.9987$). **b.**, Food intake across all groups for the duration of the experiment while on CNO. Data reported as mean \pm SEM. Significance determined by one-way ANOVA adjusted for multiple comparisons by Tukey's HSD. TLS mice (1.17 ± 0.10 g) had significantly lower food intake than Con 22°C mice (3.67 ± 0.18 g) (****, $P < 0.0001$), Con 32°C mice (3.25 ± 0.22 g)

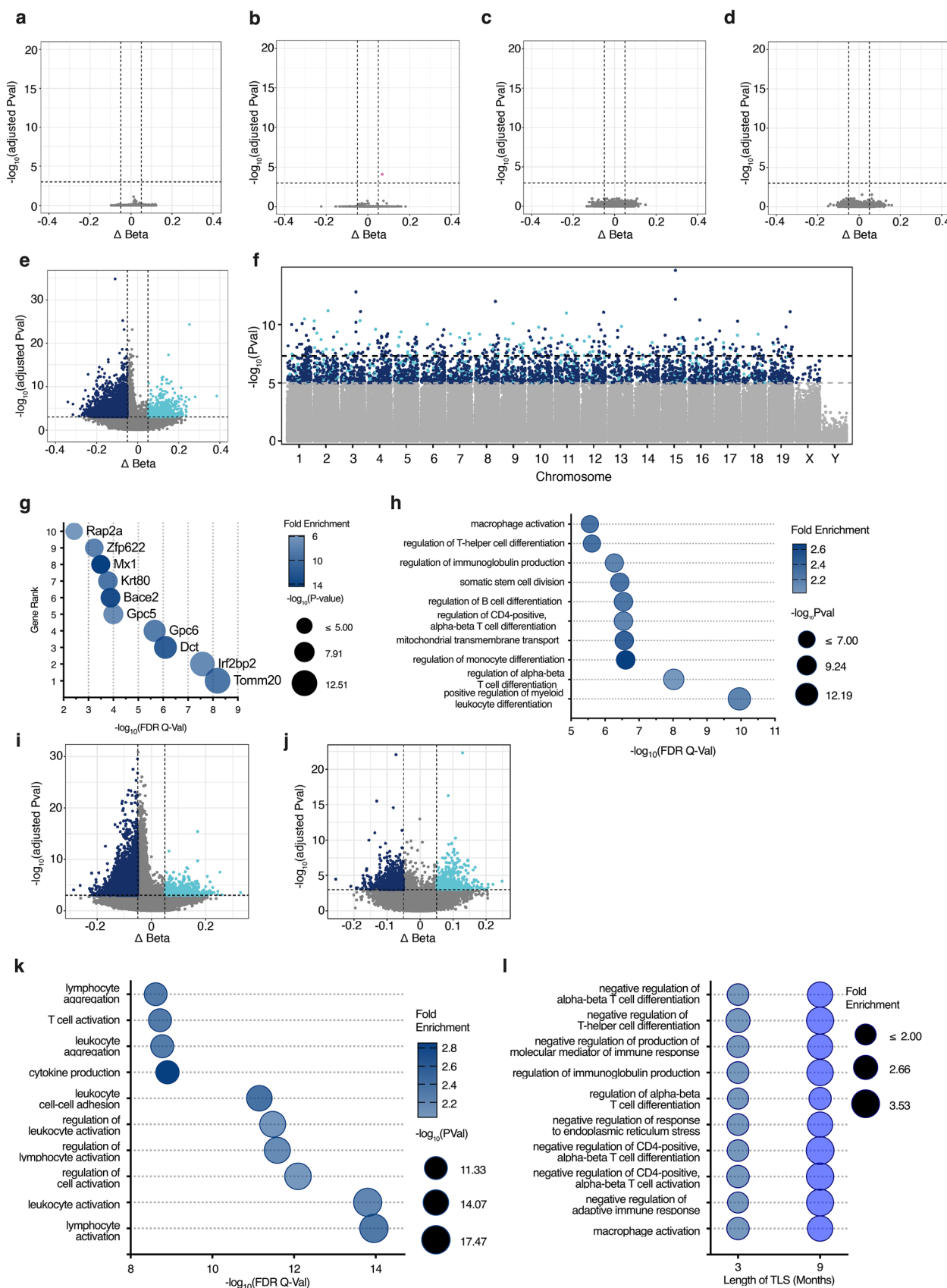
(**** $P < 0.0001$), and Stim 32°C mice (2.30 ± 0.12 g) (***, $P = 0.0003$). Importantly, TLS mice had similar food intake to CR 32°C mice (0.95 ± 0.0 (ns, $P = 0.8868$) and Stim + CR 32°C mice (0.88 ± 0.02) (ns, $P = 0.7270$). Stim + CR 32°C mice ate equivalent amounts as CR 32°C mice (ns, $P = 0.9945$), and both groups ate significantly less than Con 22°C mice (Stim + CR 32°C vs. Con 22°C mice, **** $P > 0.0001$; CR 32°C vs. Con 22°C mice, **** $P < 0.0001$), Con 32°C mice (Stim + CR 32°C vs. Con 32°C mice, **** $P > 0.0001$; CR 32°C vs. Con 32°C mice, **** $P < 0.0001$) and Stim 32°C mice (Stim + CR 32°C vs. Stim 32°C mice, **** $P > 0.0001$; CR 32°C vs. Stim 32°C mice, **** $P < 0.0001$). Con 32°C mice ate equivalent amounts as Con 22°C mice (ns, $P = 0.3588$). Stim 32°C mice ate significantly less than Con 32°C mice (** $P = 0.0062$) and Con 22°C mice (**** $P < 0.0001$). **c.**, Aggregate plot of T_b over 12 week experiment displayed over a 1 week interval of control (grey) and TLS (blue) mice. Data plotted as mean \pm s.d. **d.**, Food intake of TLS mice and Control mice while on and off CNO over duration of the experiment. **e.**, Aggregate plot of T_b over 12 week experiment displayed over a 1 week interval of Con 32°C and Stim 32°C mice. TLS mice shown in blue for reference. Data plotted as mean \pm SD. **f.**, Food-intake of Con 32°C and Stim 32°C mice while on and off CNO. **g-h.**, Characterization of CR 32°C mice, data shown as in **e-f**. **i-j.**, Characterization of Stim + CR 32°C mice, data shown as in **e-f**.



Extended Data Fig. 8 | See next page for caption.

Extended Data Fig. 8 | Analysis of potential sex-differences across experiments. **a**, Violin plot showing the distribution of ΔT_b [$^{\circ}$ C] while on CNO over the course of the longitudinal experiment in male and female TLS mice (Fig. 3). There was no significant difference (ns, $P = 0.2691$) between males (-5.115) and females (-5.559) as determined by two-sided unpaired T-test ($t = 1.131$, df = 24). **b-d**, To test for sex-differences in TLS, we compared rates of epigenetic aging using simple linear regression between **(b)** female TLS mice and female control mice **(c)** between male TLS mice and control mice, and **(d)** between male and female TLS mice. Data plotted as box plots (25th to 75th percentile) with whiskers from min-to-max with line at median. In **(b)** we found that female TLS mice ($r^2 = 0.91$, slope = 0.5352 ± 0.037) age significantly slower than female control mice ($r^2 = 0.96$, slope = 0.8404 ± 0.038) ($F = 32.72$, DFn = 1, DFd = 43, **** $P < 0.0001$). Slope reported as mean \pm standard error. In **(c)** we found that male TLS mice ($r^2 = 0.94$, slope = 0.60 ± 0.045) age significantly slower than male control mice ($r^2 = 0.96$, slope = 0.97 ± 0.05) ($F = 28.7$, DFn = 1, DFd = 26, *** $P < 0.0001$). Slope reported as mean \pm standard error. In **(d)** we found that there is no significant difference between the aging rates of female ($r^2 = 0.91$, slope = 0.5352 ± 0.037) and male TLS mice ($r^2 = 0.94$, slope = 0.60 ± 0.045) ($F = 1.141$, DFn = 1, DFd = 32, ns, $P = 0.293$). In **(e-h)** we compared the epigenetic age of male and female TLS and control mice at every timepoint using one-way ANOVA with multiple comparisons. Data plotted as box plots (25th to 75th percentile) with whiskers from min-to-max with line at median. In **(e)** we found that there were no significant differences between groups at T0 (ns, $P = 0.2467$). In **(f)** we found that there were significant differences between control females (0.438) and TLS females (0.357) (* $P = 0.011$), and between control males (0.458) and TLS males (0.362) (** $P = 0.009$). There was no significant difference between control females and control males (ns, $P = 0.831$), or between TLS females and

TLS males (ns, $P = 0.998$). In **(g)** we found that there were significant differences between control females (0.657) and TLS females (0.465) (**** $P < 0.0001$) and between control males (0.644) and TLS males (0.485) (** $P = 0.0018$). We found no significant differences between control females and control males (ns, $P = 0.971$), or between TLS females and TLS males (ns, $P = 0.93$). In **(h)** we found that there were significant differences between control females (0.869) and TLS females (0.639) (** $P = 0.002$) and between control males (1.024) and TLS males (0.706) (** $P = 0.007$). We found no significant differences between control females and control males (ns, $P = 0.112$), or between TLS females and TLS males (ns, $P = 0.719$). **i**, Violin plot showing the distribution ΔT_b [$^{\circ}$ C] while on CNO over the course of a 3-month experiment in male and female TLS mice (Figs. 2, 4). There was no significant difference (ns, $P = 0.31$) between males (-5.223) and females (-5.496) as determined by unpaired T-test ($t = 1.039$, df = 22). To test whether either sex responded differently to clamping the temperature or to caloric restriction, we compared male and female groups within each experiment using one-way ANOVA corrected for multiple comparisons with Tukey's HSD in **(j-k)**. In **(j)**, we found that there were no significant differences between T0 females (0.377) and males (0.400) (ns, $P = 0.9998$), between No Stim 22 $^{\circ}$ C (0.478) females and males (0.527) (ns, $P = 0.9322$), between TLS males (0.374) and females (0.4525) (ns, $P = 0.4795$), between No Stim 32 $^{\circ}$ C females (0.47) and males (0.476) (ns, $P > 0.9999$), and between Stim 32 $^{\circ}$ C females (0.5008) and males (0.507) (ns, $P > 0.999$). In **(k)** we found that there were no significant differences between T0 females (0.316) and T0 males (0.316) (ns, $P > 0.999$), between No Stim 22 $^{\circ}$ C females (0.484) and males (0.496) (ns, $P = 0.9998$), between CR 32 $^{\circ}$ C females (0.462) and males (0.448) (ns, $P > 0.9999$), and between Stim+CR 32 $^{\circ}$ C females (0.4755) and males (0.4861) (ns, $P = 0.9995$).



Extended Data Fig. 9 | See next page for caption.

Extended Data Fig. 9 | Differential methylation analysis. **a-e**, Volcano plots of differentially methylated regions across all groups as compared to Control 22°C mice. Differential methylation analysis was performed using the SeSAmE pipeline, which identified 183,635 genomic regions with correlated CpGs from 326,723 probes. Dashed lines represent significance thresholds as determined by DMR function, which models DNA methylation levels using mixed linear models, treating conditions as covariates, with the following thresholds (adjusted P-value $< 10^{-3}$ and $|\Delta\text{Beta}| > 0.05$). Importantly, only mice that underwent TLS had a meaningful number of differentially methylated regions as compared to Control 22°C mice after 3 months of treatment, suggesting temperature-dependent epigenetic remodeling. **a**, Control 32°C, no significantly differentially methylated regions. **b**, Stim 32°C, 1 hypermethylated region (highlighted in pink). **c**, CR 32°C, no differentially methylated regions. **d**, Stim+CR 32°C, had no differentially methylated regions. **e**, TLS, 701 significantly hypermethylated regions highlighted in light blue, 5,332 significantly hypomethylated regions highlighted in dark blue. **f**, Manhattan plot showing the 286,212 probes that mapped to the mouse genome using the SeSAmE pipeline to visualize the genomic locations of differentially methylated probes between TLS and Control 22°C mice. Lower dashed line represents the significance threshold (raw P-value $< 10^{-5}$). Probes that were significantly hypermethylated in TLS mice as compared to controls are highlighted in light blue; significantly hypomethylated probes are highlighted in dark blue. **g**, Top 10 enriched gene hits in TLS mice

as compared to Control 22°C mice after 3 months of treatment identified via Genomic Regions Enrichment of Annotations Tool (GREAT) analysis from all differentially methylated regions. **h**, Top 10 enriched biological processes in TLS mice as compared to Control 22°C mice after 3 months of treatment identified via GREAT analysis. Only biological processes with more than 10 foreground gene hits were included. **i-j**, Volcano plots of differentially methylated regions in TLS mice as compared to control mice after 6 (**i**) and 9 (**j**) months of TLS. Differential methylation analysis was performed using the SeSAmE pipeline, which identified 183,635 correlated genomic segments. Dashed lines represent significance thresholds (adjusted P-value $< 10^{-3}$ and $|\Delta\text{Beta}| > 0.05$). Significantly hypermethylated regions are highlighted in light blue; significantly hypomethylated regions are highlighted in dark blue. **i**, After 6 months of TLS, there were 567 significantly differentially hypermethylated regions and 10,614 significantly differentially hypomethylated regions. **j**, After 9 months of TLS, there were 517 significantly differentially hypermethylated regions and 871 significantly differentially hypomethylated regions. **k**, Top 10 enriched biological processes after 9 months of TLS identified via GREAT analysis. Only biological processes with more than 10 foreground gene hits were included. **l**, Shared significantly enriched biological processes after 3 and 9 months of TLS identified using GREAT analysis. Biological processes were limited to those with an FDR < 0.05 and more than 5 foreground gene hits.

Corresponding author(s): Sinisa Hrvatin

Last updated by author(s): 01/30/2025

Reporting Summary

Nature Portfolio wishes to improve the reproducibility of the work that we publish. This form provides structure for consistency and transparency in reporting. For further information on Nature Portfolio policies, see our [Editorial Policies](#) and the [Editorial Policy Checklist](#).

Statistics

For all statistical analyses, confirm that the following items are present in the figure legend, table legend, main text, or Methods section.

n/a Confirmed

- The exact sample size (n) for each experimental group/condition, given as a discrete number and unit of measurement
- A statement on whether measurements were taken from distinct samples or whether the same sample was measured repeatedly
- The statistical test(s) used AND whether they are one- or two-sided
Only common tests should be described solely by name; describe more complex techniques in the Methods section.
- A description of all covariates tested
- A description of any assumptions or corrections, such as tests of normality and adjustment for multiple comparisons
- A full description of the statistical parameters including central tendency (e.g. means) or other basic estimates (e.g. regression coefficient) AND variation (e.g. standard deviation) or associated estimates of uncertainty (e.g. confidence intervals)
- For null hypothesis testing, the test statistic (e.g. F , t , r) with confidence intervals, effect sizes, degrees of freedom and P value noted
Give P values as exact values whenever suitable.
- For Bayesian analysis, information on the choice of priors and Markov chain Monte Carlo settings
- For hierarchical and complex designs, identification of the appropriate level for tests and full reporting of outcomes
- Estimates of effect sizes (e.g. Cohen's d , Pearson's r), indicating how they were calculated

Our web collection on [statistics for biologists](#) contains articles on many of the points above.

Software and code

Policy information about [availability of computer code](#)

Data collection

For long-term temperature monitoring, mice were implanted with UID temperature microchips (UID Cat# UCT2112) and cages were places on the UID Mouse Matrix reader plate. For metabolic measurements, Mice were implanted abdominally with telemetric temperature probes (Starr Life Science VV-EMITT-G2) and placed in the Sable Systems Promethion Core Metabolic System. For clamping temperature, mice were housed in thermoneutral temperature in a Powers Scientific Incubator (IT54SD). For tissue processing, DNA was extracted using DNeasy Blood and Tissue kits (Qiagen #69506), RNA was extracted using RNeasy mini kits (Qjagen #74104). For epigenetic clock analysis, DNA was bisulfite converted using zymo EZ DNA methylation kit (D5004) and was run on the custom Illumina HorvathMammalMethylChip320. For RNAseq analysis, libraries were prepared using the NEBNext Ultra II kit and sequenced on a NovaSeq6000.

Data analysis

Most analysis was performed in R, Python, and GraphPad Prism. Statistical analysis of the thermoregulatory system was performed as previously described with publicly available code from G.A. Sunagawa, 2016. R code of all epigenetic clocks can be found in the MammalMethylClock R package. Differential methylation analysis was performed using the SeSaMe pipeline (v1.16) . Gene enrichment and biologicalprocesses analysis were performed using the Genomic Regions Enrichment of Annotations Tool (GREAT v.4.0.4.). RNAseq reads were aligned to the mm10 reference mouse genome using STAR v2.7.10. Transcriptomic clock analysis was performed as previously described by A. Tyshkovskiy (2019 and 2023) using edgeR(v 4.2.0) (Robinson, 2010). Differential gene expression was performed using DESeq2 (v1.46)

For manuscripts utilizing custom algorithms or software that are central to the research but not yet described in published literature, software must be made available to editors and reviewers. We strongly encourage code deposition in a community repository (e.g. GitHub). See the Nature Portfolio [guidelines for submitting code & software](#) for further information.

Data

Policy information about [availability of data](#)

All manuscripts must include a [data availability statement](#). This statement should provide the following information, where applicable:

- Accession codes, unique identifiers, or web links for publicly available datasets
- A description of any restrictions on data availability
- For clinical datasets or third party data, please ensure that the statement adheres to our [policy](#)

All raw and processed methylation data is deposited and available at GEO accession (Geo accession #282499, 282659, 282661). Raw and processed RNA-seq data is deposited and available at GEO accession (GSE288355). All additional source data available in supplementary information files. If there is any additional data missing from repositories and/or supplemental information files, data is available from corresponding author upon reasonable request. RNA seq reads were aligned to the mm10 reference mouse genome using STAR v2.7.10. The mm10 reference genome is available at NCBI RefSeq assembly (GCF 000001635.20).

Research involving human participants, their data, or biological material

Policy information about studies with [human participants or human data](#). See also policy information about [sex, gender \(identity/presentation\), and sexual orientation](#) and [race, ethnicity and racism](#).

Reporting on sex and gender

n/a

Reporting on race, ethnicity, or other socially relevant groupings

n/a

Population characteristics

n/a

Recruitment

n/a

Ethics oversight

n/a

Note that full information on the approval of the study protocol must also be provided in the manuscript.

Field-specific reporting

Please select the one below that is the best fit for your research. If you are not sure, read the appropriate sections before making your selection.

Life sciences

Behavioural & social sciences

Ecological, evolutionary & environmental sciences

For a reference copy of the document with all sections, see nature.com/documents/nr-reporting-summary-flat.pdf

Life sciences study design

All studies must disclose on these points even when the disclosure is negative.

Sample size

Sample size was predetermined based on power analyses from previously reported epigenetic clocks [21], and estimates based on effect size of hibernation on epigenetic age in other species [25].

Data exclusions

Pre-established criteria were used for data inclusion/exclusion. Mainly, in long-term epigenetic experiments, only animals from which we were able to extract sufficient blood for downstream processing were included at each measured time point.

Replication

Each experiment was performed a single time with multiple animals (numbers indicated in manuscript). Data is displayed as individual points indicating the distribution of results throughout the manuscript. In independent experiments that overlapped in groups (i.e. TLS mice in short-term and long-term experiments), the results were in agreement.

Randomization

Assignment of age- and gender-matched mice to different surgical and experimental groups was random.

Blinding

All epigenetic clock analyses were performed blinded to group. Frailty measurements were performed blinded to group.

Reporting for specific materials, systems and methods

We require information from authors about some types of materials, experimental systems and methods used in many studies. Here, indicate whether each material, system or method listed is relevant to your study. If you are not sure if a list item applies to your research, read the appropriate section before selecting a response.

Materials & experimental systems

n/a	Involved in the study
<input checked="" type="checkbox"/>	Antibodies
<input checked="" type="checkbox"/>	Eukaryotic cell lines
<input checked="" type="checkbox"/>	Palaeontology and archaeology
<input type="checkbox"/>	Animals and other organisms
<input checked="" type="checkbox"/>	Clinical data
<input checked="" type="checkbox"/>	Dual use research of concern
<input checked="" type="checkbox"/>	Plants

Methods

n/a	Involved in the study
<input checked="" type="checkbox"/>	ChIP-seq
<input checked="" type="checkbox"/>	Flow cytometry
<input checked="" type="checkbox"/>	MRI-based neuroimaging

Animals and other research organisms

Policy information about [studies involving animals; ARRIVE guidelines](#) recommended for reporting animal research, and [Sex and Gender in Research](#)

Laboratory animals

All experiments were performed using adult C57BL/6J mice (Jackson laboratory #000664). Sample size was predetermined based on power analyses from previously reported epigenetic clocks[21], and estimates based on effect size of hibernation on epigenetic age in other species[25]. Unless otherwise noted, all groups contained equal numbers of age-matched male and female mice randomly assigned to experimental groups before surgery. Across all experiments, mice were between 16-20 weeks old at the start of all experiments.). Unless otherwise noted, all mice were group-housed at 22°C under a standard 12 h light/dark cycle and fed ad libitum. Relative humidity was maintained at 30-70% across all experiments.

Wild animals

This study did not involve wild animals.

Reporting on sex

All experiments started with equal numbers of both male and female subjects unless otherwise stated. We've include the sample size of male and female mice in each experiment, as well as performed additional analyses looking for sex-differences.

Field-collected samples

This study did not involve samples collected in the field.

Ethics oversight

Experiments performed at Harvard Medical School were approved by the National Institute of Health and Harvard Medical School Institutional Animal Care and use Committee. Experiments performed at the Whitehead Institute at the Massachusetts Institute of Technology were approved by the National Institute of Health and the Division of Comparative Medicine and the Committee on Animal Care. All experiments followed ethical guidelines described in the US National Institutes of Health Guide for the Care and Use of Laboratory Animals.

Note that full information on the approval of the study protocol must also be provided in the manuscript.

Plants

Seed stocks

n/a

Novel plant genotypes

n/a

Authentication

n/a